Translational Research 295 (2026) 31–49

Contents lists available at ScienceDirect

Translational Research

journal homepage: www.elsevier.com/locate/trsl

Integrated RNA sequencing and in vivo biosensor imaging define the early pathogenic cascade of Duchenne muscular dystrophy

Elena Cannone [a], Martina La Spina [b], Barbara Gnutti [a], Chiara Tesoriero [c], Silvia Castagnaro [b], Chiara Tobia [a], Luca La Via [a], Patrizia Sabatelli [d,e], Cesare Faldini [e,f], Giuseppe Fiume [g], Andrea Vettori [c], Dario Finazzi [a], Massimo Gennarelli [a], Chiara Magri [a,1,*], Marco Schiavone [a,1,*]

[a] Department of Molecular and Translational Medicine, University of Brescia, Brescia, Italy
[b] Department of Biomedical Sciences, University of Padua, Padua, Italy
[c] Department of Biotechnology, University of Verona, Verona, Italy
[d] Institute of Molecular Genetics, National Research Center (CNR), Bologna, Italy
[e] IRCCS Orthopedic Institute Rizzoli, Bologna, Italy
[f] Department of Biomedical and Neuromotor Science, University of Bologna, Bologna, Italy
[g] Department of Experimental and Clinical Medicine, University Magna Græcia of Catanzaro, Catanzaro, Italy

ARTICLE INFO

Keywords:
Duchenne muscular dystrophy
RNA sequencing
Zebrafish
Human myoblasts
Human myotubes
Zebrafish biosensors
Live imaging

ABSTRACT

Duchenne muscular dystrophy (DMD) is a lethal muscle disease caused by loss of dystrophin, and characterized by progressive muscle wasting, with massive replacement of muscle fibers with adipose tissue. Yet, the early molecular events that initiate pathology remain poorly defined. Here, we combined longitudinal RNA sequencing of *sapje* dystrophic zebrafish (a single-mutation vertebrate model of human DMD characterized by a severe phenotype), transcriptomic profiling of human DMD myoblasts and myotubes, and functional *in vivo* imaging using pathway-specific zebrafish biosensors to reconstruct the cascade of events triggered by dystrophin deficiency. We observed that the earliest stages of disease are characterized by marked downregulation of genes controlling cytosolic Ca^{2+} homeostasis, mitochondrial function and organization, and Pax3/Mef2a/Srf-mediated transcriptional programs essential for satellite cell maintenance and muscle differentiation. These early deficits precede robust but ineffective regenerative and metabolic compensatory responses, accompanied by extracellular matrix remodeling and TGFβ activation. At advanced stages, both *sapje* zebrafish and human DMD myotubes converge on profound mitochondrial dysfunction, impaired cell-cycle control, and chronic inflammation signaling. Live imaging of *sapje* zebrafish biosensors validated these transcriptomic signatures, revealing reduced Notch, Bmp, Shh, Hif-1a and Wnt signaling, along with aberrant TGFβ activity and disrupted mitochondrial dynamics *in vivo*. Together, these findings identify a conserved temporal sequence linking early Ca^{2+} dysregulation to mitochondrial failure, satellite cell hyperactivation, and fibrotic remodeling, providing mechanistic insights and therapeutic targets for early intervention in DMD patients.

Introduction

Duchenne muscular dystrophy (DMD) is a severe X-linked muscle disorder characterized by progressive muscle wasting and fibrosis, ultimately leading to loss of skeletal muscle function and death from cardiac or respiratory failure.[1–3] DMD results from mutations in the dystrophin-encoding *DMD* gene located on the short arm of the X chromosome (Xp21). Most mutations are large deletions or duplications, although nonsense variants and deletions affecting the transcriptional start site also occur.[4,5] Complete loss of the full-length Dp427 isoform causes DMD, while in-frame mutations that preserve partial dystrophin function generally lead to the milder Becker muscular dystrophy (BMD).

Dystrophin is a large structural protein located beneath the sarcolemma in both skeletal and cardiac striated muscle fibers, where it

* Corresponding authors.
E-mail addresses: chiara.magri@unibs.it (C. Magri), marco.schiavone@unibs.it (M. Schiavone).
[1] These authors contributed equally to this work

https://doi.org/10.1016/j.trsl.2026.06.007
Received 16 December 2025; Received in revised form 27 April 2026; Accepted 10 June 2026
Available online 11 June 2026

functions as a mechanical stabilizer and signaling scaffold. The full-length protein consists of an N-terminal actin-binding domain, multiple central rod domains that interact with nitric oxide synthase (NOS); and a C-terminal domain that associates with components of the dystrophin-associated protein complex (DAPC).[6–9] This complex architecture links the cytoskeleton to the extracellular matrix, forming a mechanical axis that distributes force and dissipates contractile stress during muscle activity.[10] Beyond their structural role, dystrophin and DAPC regulate the activity of multiple signaling pathways essential for muscle homeostasis. For example, dystrophin anchors the neuronal NOS at the sarcolemma to modulate vasodilation, and its presence in activated muscle stem cells (MuSCs) is required for proper asymmetric division and myogenic differentiation.[11,12]

Loss of dystrophin renders the sarcolemma fragile and prone to contraction-induced damage. These membrane damages initiate a cascade of detrimental secondary events that progressively lead to muscle fiber death. An abnormal and sustained increase in intracellular Ca^{2+} levels, arising from membrane tears and leaky channels, promotes reactive oxygen species (ROS) production and mitochondrial dysfunction, impairing energy metabolism and muscle repair.[3,13–15] Repeated cycles of muscle damage and cytoplasmic leakage further provoke chronic inflammation, macrophage infiltration, and progressive muscle necrosis.

Emerging evidence indicates that dystrophin deficiency in quiescent muscle satellite cells (MuSCs) impairs their asymmetric division and myogenic differentiation, promoting their hyperactivation and generating myoblasts that proliferate excessively but fail to properly differentiate and fuse to form normal muscle fibers.[16–18] Along with chronic inflammation, these defects contribute to the progressive replacement of muscle tissue by fibrotic and adipose deposits, driven in part by the activation of fibro-adipogenic progenitors (FAPs).[19,20] Moreover, dystrophin and several interactors, such as utrophin, dysferlin, and calpain-3, are functional constituents of the myoblast centrosome, and their absence leads to centrosome amplification, misorientation, nuclear abnormalities, and impaired microtubule nucleation, further hindering differentiation.[21] Although secondary events following membrane damage are well described, the early molecular cascade of DMD pathogenesis remains incompletely defined.

The zebrafish (*Danio rerio*) is a robust vertebrate model for studying muscular dystrophies due to its conservation of genes and pathways essential for muscle biology, including orthologs of the *DMD* gene and other DAPC components. The *sapje* mutant ($dmd^{ta222a/ta222a}$) closely recapitulates key hallmarks of human DMD, including sarcolemma fragility, Ca^{2+} dysregulation, impaired force generation, and progressive muscle degeneration.[22–24] Notably, zebrafish complete muscle development by 2 days post-fertilization (dpf)[25] enabling analysis of early transcriptomic alterations that precede tissue damage.

In this study, we analyzed gene expression in *sapje* zebrafish profiles at 2, 5, and 8 dpf to define early and late transcriptomic alterations associated with dystrophin loss and to clarify the initial molecular steps of DMD. To enhance translational relevance, we compared transcriptomic zebrafish datasets with RNA-seq profiles from DMD patient-derived myoblasts and myotubes, enabling evaluation of conserved dysregulated pathways and cross-validation of potential biomarkers and therapeutic targets, across developmental and disease contexts. While zebrafish provide access to early, causative disease events before muscle degeneration, patient-derived cells model chronic pathological states characterized by impaired regeneration and inflammation.

As transcriptomic data provide only a snapshot of molecular alterations without revealing upstream regulatory activity or physiological consequences, we integrated these analyses with *in vivo* imaging of *sapje* biosensors generated to monitor the real-time activity of signaling pathways involved in muscle repair, differentiation, and inflammation. Finally, we have performed functional assays to further validate key transcriptomic data. Together, this integrative approach enables a more comprehensive reconstruction of the molecular cascade driving the DMD pathogenesis.

Results

Transcriptome analysis of sapje zebrafish

To elucidate the sequence of molecular events underlying DMD pathogenesis and to identify early mechanisms affected by dystrophin loss, we performed bulk RNA-seq profiling of *sapje* and wild-type (WT) zebrafish at 2, 5, and 8 days post-fertilization (dpf). Developmental and pathological differences between WT and *sapje* zebrafish at these stages are summarized in Table 1.[22,23,26,27] RNA was extracted from 22 pooled samples (four WT and four *sapje* pools at 2 and 5 dpf, and three WT and three *sapje* pools at 8 dpf), each containing at least 30 zebrafish embryos/larvae, and subjected to RNA sequencing.

Longitudinal analysis of WT zebrafish revealed 8,615 genes whose expression changed significantly over time, with 4,670 progressively upregulated and 3,945 downregulated between 2 and 8 dpf (Supplementary Table 1). Gene Set Enrichment Analysis (GSEA) identified 72 enriched biological processes and Reactome pathways, including sensory and hormonal responses, starvation response, and cytochrome P450-mediated metabolism (Supplementary Table 2). We also observed progressive upregulation of TOR signaling, along with pathways involved in neuronal development, synaptic maturation, and visual perception, consistent with physiological maturation of metabolic and nervous systems during larval development.[28–31]

Conversely, genes associated with 323 GO Biological Process and Reactome pathways, including cell cycle progression, DNA replication and repair, chromatin remodeling, RNA processing, epigenetic regulation, tissue differentiation, were progressively downregulated, reflecting the expected transition from a proliferative embryonic state to tissue differentiation.[32,33]

To identify genes with different longitudinal expression trajectories between WT and *sapje* zebrafish, we tested the interaction between genotype and developmental stage using a generalized linear model. This analysis did not reveal significant single-gene differences (Supplementary Table 3). However, GSEA, which is more sensitive in capturing coordinated shifts across functional gene sets even in the absence of strong single-gene signals, identified 16 enriched biological processes related to muscle development and cell cycle regulation (Supplementary Table 4), indicating altered temporal regulation rather than static gene expression differences. Muscle-related pathways declined more slowly or increased more rapidly in *sapje* larvae, consistent with premature activation or delayed repression of programs relevant to early DMD pathology. Enrichment of the "cell cycle G2/M phase transition" pathway further supports an altered balance between proliferation and

Table 1
Muscle developmental differences between WT and *sapje* zebrafish.

	2 dpf	5 dpf	8dpf
WT	muscle development is fully completed, and muscles are functional	zebrafish larvae can swim and feed autonomously, and the innate immune system is fully developed	zebrafish larvae move faster and muscle volume increases
sapje	severe muscle development and first macrophage infiltration appear at this stage	muscles try to activate compensatory mechanisms to repair damages but both degeneration/ regeneration cycles and macrophage infiltration start to be chronic, a little increase of extracellular matrix deposition and muscle fibrosis starts to be visible	muscle damage is irreversible, muscle fibrosis is visible, motor behavior is totally compromised and >75% fish die

differentiation in muscle precursor cells, consistent with aberrant regenerative responses.[34]

To better understand mechanisms affected by dystrophin loss, we performed three separate cross-sectional analyses, comparing gene expression levels between WT and *sapje* zebrafish at 2, 5, and 8 dpf, using Wald tests to identify differentially expressed genes (DEGs) within each age-matched group. We identified 2,922 DEGs at 2 dpf (1,373 upregulated; 1,549 downregulated), 756 at 5 dpf (428 upregulated; 328 downregulated), and 103 at 8 dpf (28 upregulated; 75 downregulated) (Fig. 1A; Supplementary Table 5). The reduced number of DEGs detected at 8 dpf likely reflects the lower number of biological replicates (three biological replicates instead of four), rather than reduced transcriptional dysregulation. Fourteen genes were differentially expressed at all time points, and 267 were shared between 5 and 8 dpf (Fig. 1A), significantly exceeding random overlap expectations, thus indicating that these changes represent core components of the DMD phenotype. Among the 14 DEGs consistently altered at all stages, *dmd* was persistently downregulated in *sapje* larvae, together with other seven genes mainly involved in inflammation (*lgmn* and *CR847936.6*, a novel uncharacterized gene regulated by the glucocorticoid receptor), mitosis and cytoskeleton organization (*pcnp, afap1l1b*, and *nsfl1c*), collagen hydroxylation (*plod3*), and oxidative phosphorylation (*sdhc*) (Fig. 1C). Conversely, six genes were consistently upregulated, including pro-inflammatory (*mmp2*), pro-myogenic (*mustn1b, mtus1b*, and *myog*), and genes involved in Ca^{2+}- dependent cardiac contraction (*tnnt2e*, and *myl10*). These expression patterns indicate that dysregulation of Ca^{2+} homeostasis, mitochondrial dysfunction, and inflammation emerge early and persist throughout disease progression.

GSEA revealed that the number of aberrant pathways increased progressively over time, reflecting the gradual worsening of disease (Supplementary Tables 6, 7, and 8).

At 2 dpf, we observed strong downregulation of gene sets involved in the i) regulation and transport of cytosolic Ca^{2+}, and ii) skeletal and cardiac muscle contraction (Fig. 2; Supplementary Table 6). The absence of upregulated pathways at this stage suggests an early functional deficit preceding the activation of compensatory responses.

At 5 dpf, a marked upregulation of pathways associated with muscle development, oxidative phosphorylation, skeletal and cardiac muscle contraction, protein folding, and extracellular matrix (ECM) organization was observed (Fig. 2; Supplementary Table 7). These changes likely

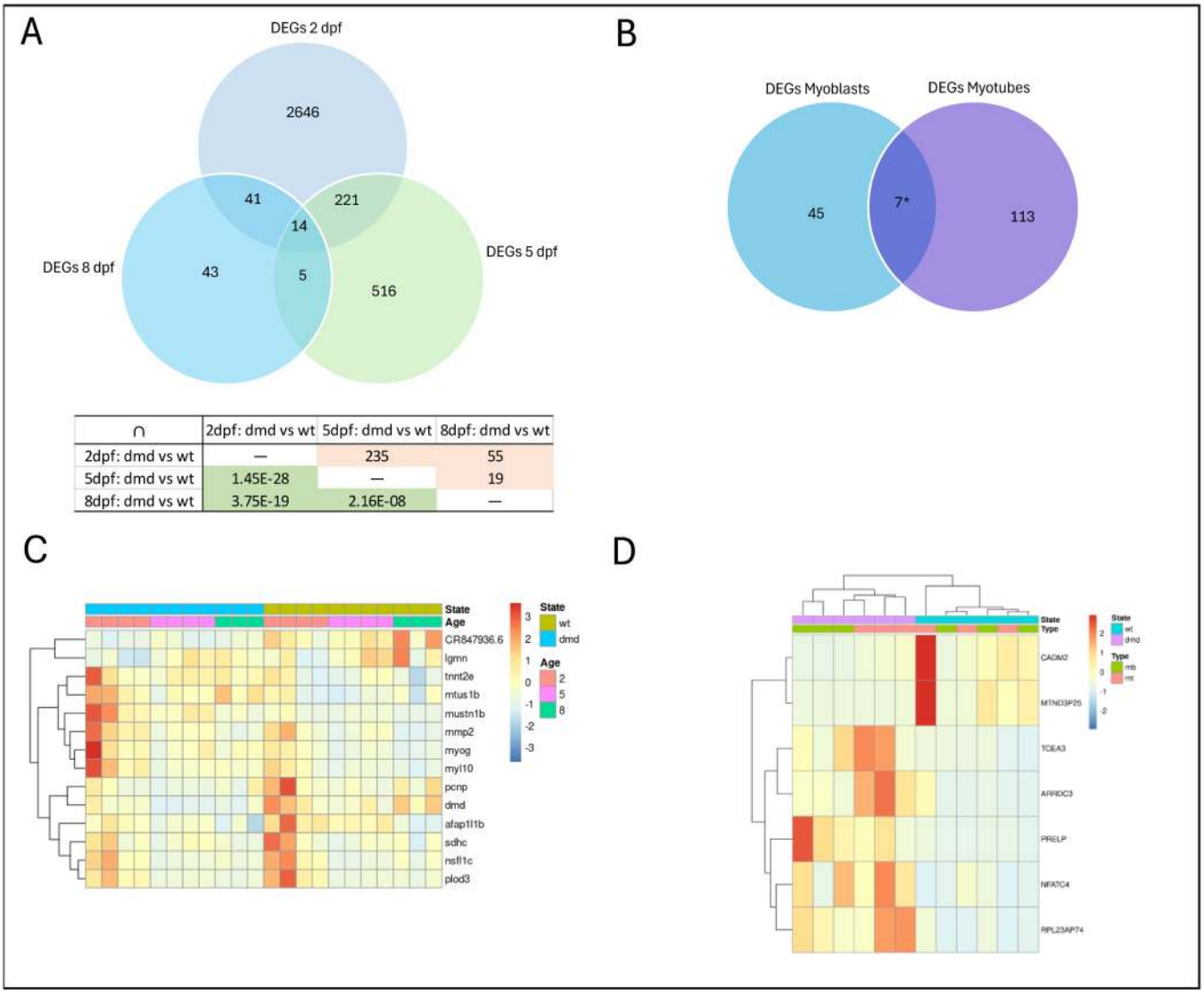

∩	2dpf: dmd vs wt	5dpf: dmd vs wt	8dpf: dmd vs wt
2dpf: dmd vs wt	—	235	55
5dpf: dmd vs wt	1.45E-28	—	19
8dpf: dmd vs wt	3.75E-19	2.16E-08	—

Fig. 1. Summary of the differential expression analyses performed in *D. rerio* and Human cell lines. A) Number of overlapping DEGs in the three comparisons in zebrafish, with the matrix showing in the upper corner the number of DEGs common to more than one comparison and in the lower corner the p-values of the hypergeometric test. B) Number of overlapping DEGs in the two human cell lines. C) Heatmap of the 14 genes that are differentially expressed in all three zebrafish comparisons (Z-score normalized values are reported). D) Heatmap of the seven genes that are DEGs both in myoblasts and myotubes.

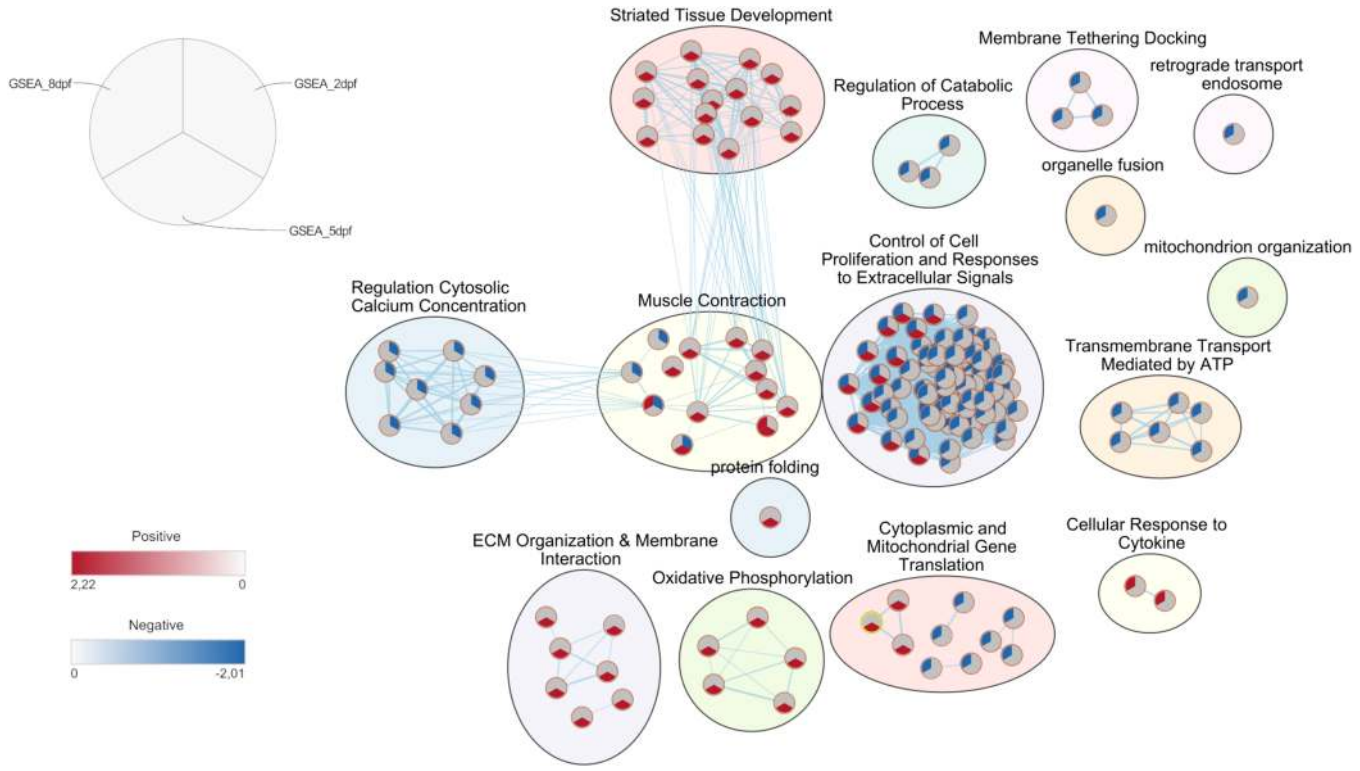

Fig. 2. Enrichment map visualization of the GSEA enrichment analysis performed on the RNA sequencing dataset in Zebrafish. Each circle (node) represents a gene set (GO:Biological Process) or Reactome Pathway. Red slices are pathways enriched for genes up-regulated and blue slices are pathways enriched for genes down-regulated in dmd embryos compared with WT. The position of the colored slice depends on the development stage. Pathways (nodes) are connected when they overlap (i.e., they have genes in common), with line width corresponding to the number of shared genes (light blue lines).

represent compensatory but ineffective attempts by the organism to sustain muscle integrity and initiate regeneration, accompanied by early fibrotic remodeling.[35,36]

At 8 dpf, upregulated pathways sharply declined. The remaining upregulated gene sets were associated to inflammatory response and cytokine-mediated signaling pathways (Fig. 2; Supplementary Table 8), along with persistent activation of "muscle system process" genes. The overwhelming trend at 8 dpf was a marked downregulation of pathways related to cell cycle and DNA replication, immune responses (especially NF-kB dependent response), mitochondria translation, organization and metabolism, metabolic processes, and proteasome-mediated protein catabolism. Together, these findings indicate systemic failure of regenerative and homeostatic mechanisms at advanced disease stages.

GSEA of Transcription Factor (TF) target genes showed significant

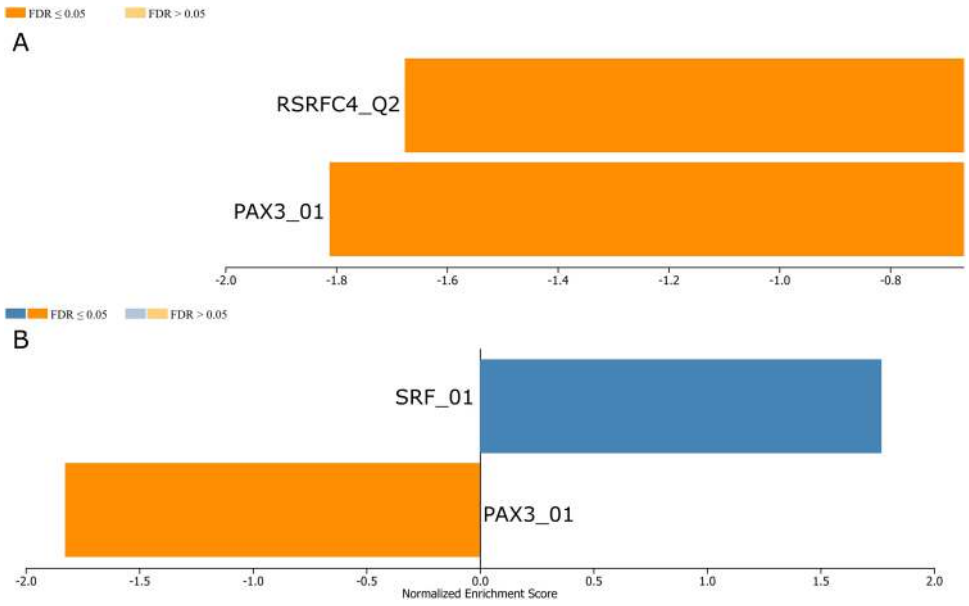

Fig. 3. Bar Chart of Transcription Factor (TF) Targets enrichment analysis. A) TF target gene-sets found enriched at 2 dpf. B) TF target gene-sets found enriched at 5 dpf. The orange rectangle means gene down-regulation, the blue rectangle means gene up-regulation.

repression of Pax3 and Mef2a target genes at 2 dpf (Fig. 3). Pax3 is critical for satellite cell maintenance, migration, and early myogenic commitment,[37–39] while Mef2a regulates Ca^{2+}-dependent muscle gene expression.[40] Downregulation of Pax3 target genes persisted at 5 dpf, whereas Srf target genes were upregulated at this stage, consistent with activation of stress-responsive and compensatory transcriptional programs.[41] Notably, none of the TFs themselves were differentially expressed, suggesting post-transcriptional regulation.

Transcriptome analysis of human cell lines

We next analyzed transcriptomes of myoblasts and myotubes from DMD patients and healthy donors.

In myoblasts, we identified 51 DEGs (33 upregulated; 18 downregulated), and in myotubes, 120 DEGs (60 upregulated; 60 downregulated). Seven DEGs (*NFATC4, ARRDC3, CADM2, PRELP, TCEA3, RPL23AP74, MTND3P25*), involved in inflammation, apoptosis, ECM remodeling, cell-cycle regulation, and oxidative phosphorylation (OXPHOS), were differentially expressed in both cell types: a number 20.31-fold higher than that expected by chance ($p = 4.9 \times 10^{-8}$; Fig. 1B, D; Supplementary Table 9).

In myoblasts, the predominant alterations were downregulated pathways associated with cell-cycle regulation, DNA replication and repair, chromosome dynamics, and telomere maintenance (Fig. 4; Supplementary Table 10). This suggested impaired proliferation and genomic stability, consistent with reduced regenerative capacity. This deficit in regenerative potential is shared with zebrafish, showing similar pathway downregulation at 8 dpf. Beyond cell cycle and DNA, we also identified a significant downregulation of pathways related to muscle development and contraction, suggesting reduced myogenic commitment of myoblasts even before differentiation into myotubes. Gene sets related to mitochondrial function, RNA metabolism, and immune signaling were also suppressed, indicating mitochondrial dysfunction, deficit in energy production, and dysregulated inflammatory responses. Conversely, we observed few upregulated pathways, mainly involved in ECM remodeling and catabolic processes. Increased ECM-related gene expression could reflect early fibrotic remodeling or microenvironmental adaptation to cellular stress. These observations were observed also in *sapje* zebrafish, reaching a peak at 5 dpf. On the contrary, upregulation of genes involved in the catabolism of Glycosaminoglycan, Aminoglycan and Sulfur compounds could indicate increased cellular turnover or an attempt to remove damaged components.

In myotubes, all enriched pathways were downregulated (Fig. 4; Supplementary Table 11). These pathways are mainly related to muscle structure, contraction, and development, revealing severe defects in myotube formation and function that align with clinical muscle weakness in DMD. This directly reflects the muscle weakness and degeneration observed in DMD patients. Downregulation of genes involved in mitochondrial processes and energy metabolism indicates pronounced mitochondrial dysfunction in mature muscle cells. We also observed a strong downregulation of genes involved in lipid and steroid metabolism, suggesting compromised membrane integrity and cellular homeostasis. Further downregulation of genes involved in the cell-cycle, although less extensive than in myoblasts, could reflect aberrant regenerative attempts or impaired terminal differentiation. Notably, no upregulated pathways were detected, suggesting a globally repressed transcriptional state, possibly influenced by the absence of the physiological muscle microenvironment.[42]

A cross-comparison of myoblasts and myotubes, revealed shared defects in pathways related to muscle contraction, filament sliding, and muscle development, suggesting that functional deficits originate at early precursor stages and worsen with differentiation. Mitochondrial pathways were downregulated in both cell types, indicating pervasive mitochondrial dysfunction and defects in energy production. Core protein-degradation pathways (such as SCF- and APC/C-mediated degradation) and several ubiquitin-dependent pathways were downregulated in both models, suggesting impaired protein turnover and

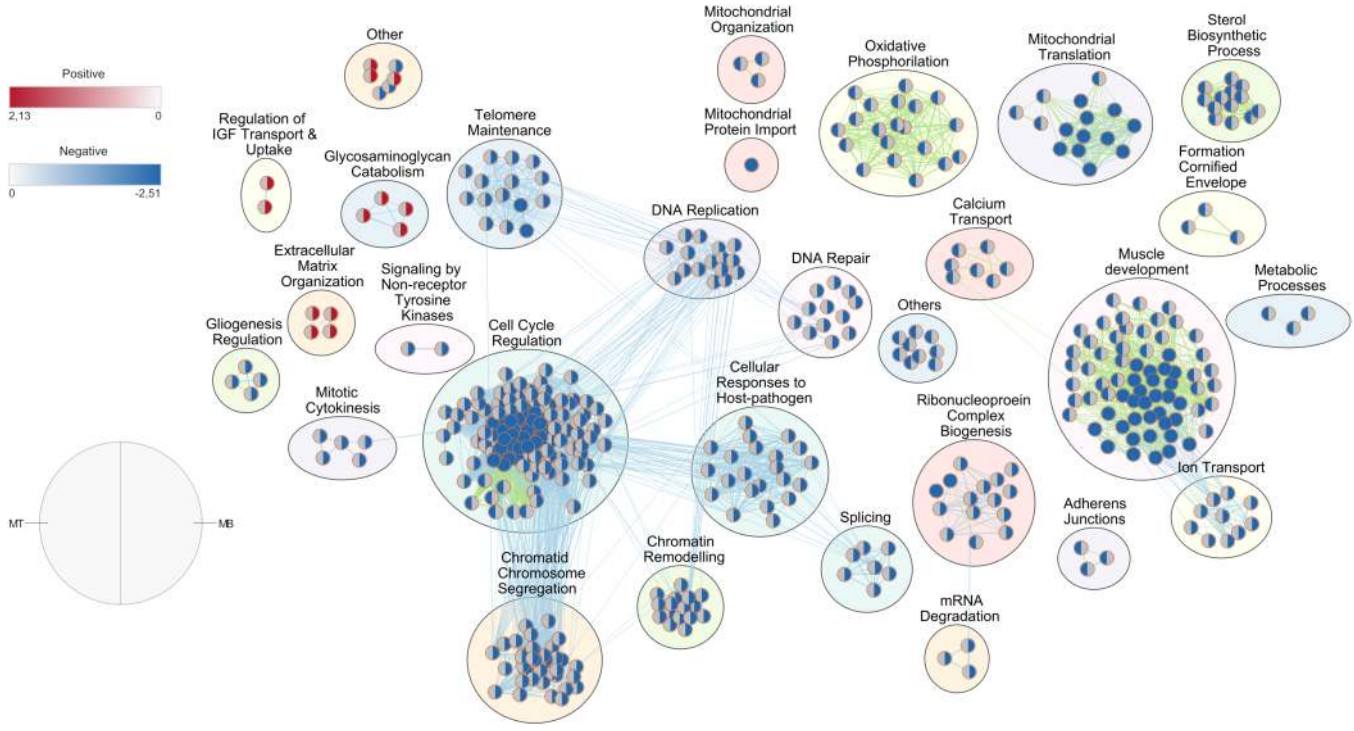

Fig. 4. Enrichment map visualization of the GSEA enrichment analysis performed on the RNA sequencing dataset of human myoblast cell-lines (MB) and differentiated myotubes (MT). Each circle (node) represents a gene set (GO:Biological Process) or Reactome Pathway. Red slices are pathways enriched for genes up-regulated and blue slices are pathways enriched for genes down-regulated in cells of DMD patients compared to healthy controls. Left colored slices are referred to MT, whereas the right ones to MB. Pathways (nodes) are connected when they overlap, with line width corresponding to the number of shared genes.

accumulation of aberrant proteins. Moreover, NIK (NFκB-inducing kinase) and FCERI-mediated NF-kB activation were also downregulated, indicating altered inflammatory signaling.

TF-target GSEA revealed enrichment of downregulated E2F target genes in myoblasts (Supplementary Fig. 3), consistent with impaired proliferation. Targets of ZBTB14 and SF1, two regulators of transcriptional repression and RNA maturation, were also suppressed, aligning with downregulation of genes involved in pre-mRNA splicing (such as, UBP1, ELK1). In myotubes, downregulation of MEF2 target genes mirrored the suppression observed in *sapje* zebrafish at 2 dpf.

Integrated analysis of zebrafish and human RNA-sequencing data

Among 21,973 human/zebrafish ortholog pairs identified using Ensembl, 12,462 were analyzable across datasets. In line with the inherent biological differences between developing larvae and human adult-derived cells, very few shared DEGs were identified across species (Supplementary Table 12). The most notable overlap occurred between human myotubes and zebrafish at 2 dpf, comprising 26 human DEGs corresponding to 30 zebrafish orthologs. Notably, two of these genes (*dmd,* as expected*,* and *myog*) were altered at multiple zebrafish stages (2, 5 and 8 dpf). *DMD* gene was consistently downregulated both in DMD patient cell lines and in *sapje* zebrafish, whereas *MYOG* gene was downregulated in human DMD myotubes but upregulated in *sapje* zebrafish at all stages, consistent with hyperproliferation of myoblasts that fail to differentiate or regenerate effectively.

Although gene-level overlap was modest, pathway-level comparisons revealed a more robust functional convergence. Pathways suppressed in human myoblasts partially mirrored those downregulated in *sapje* zebrafish at late disease stages (8 dpf), especially those involved in cell-cycle progression, DNA replication, and chromosome maintenance. This shared signature points toward a conservative impairment in the regenerative capacity of muscle cells across species.

Human myotubes displayed similarities to the advanced transcriptomic state of zebrafish at 8 dpf, characterized by extensive repression of muscle structure, sarcomere organization, and mitochondrial-energy pathways, and absence of compensatory responses. While these findings highlight conserved pathogenic nodes, they should be interpreted with caution given the distinct developmental contexts and cellular heterogeneity inherent to each model.

Live imaging of sapje zebrafish biosensors

Despite providing broad insights into the sequence of altered biological pathways during DMD pathogenesis, transcriptomic data alone do not fully reveal the activity of crucial signaling pathways controlling cellular processes like muscle regeneration, differentiation, and the inflammatory response. To overcome this issue, we integrated RNA-seq with *in vivo* imaging of fluorescent *sapje* biosensors generated to monitor the dynamics of crucial signaling pathways. Specifically, we generated fluorescence *sapje* biosensors expressing GFP or mCherry under the control of pathway-responsive promoter elements for Shh, Notch, Tgfβ, Wnt, Bmp, and Hif-1α signaling pathways.[43] Their activity was observed and quantified at 2 and 5 dpf in WT and *sapje* larvae. We observed a significant and stable reduction in Shh, Bmp, Hif-1α, and Notch activity in *sapje* from early stages of disease progression (Figs. 5A, B, D; Fig. 6B, d'-g'; Supplementary Fig. 4). These pathways are essential for MuSCs self-renewal, asymmetric division, and commitment to first myoblasts and then multinucleated myofibers.[19,44–49] Conversely, canonical Wnt was unaffected at 2 dpf but showed a decreasing trend at 5 dpf (Fig. 5C, e-f), consistent with impaired regeneration.

Tgfβ signaling activity was markedly increased and relocalized from myonuclei to small-nuclei cells (Fig. 6B, a'-c', h'). Together with increased macrophage infiltration observed using *sapje;tg(mpeg:GFP)* biosensor (Fig. 7) and previous TEM evidence[50] these findings indicate early, severe fibrosis.[51]

Furthermore, a mitochondrial-targeted *sapje* biosensor, the *sapje;tg (COXVIII:GFP)*, revealed severely disrupted mitochondrial network, with marked accumulation of fragmented mitochondria at lesion sites (Fig. 8), suggesting enhanced mitochondrial fission or dysfunction.

In vivo observations of both signaling pathways and mitochondrial dynamics align with transcriptomic data of *sapje* zebrafish.

Functional and physiological validation of RNA-sequencing in living sapje zebrafish

We first confirmed whether the reduced activity of signaling pathways involved in muscle development and MuSCs differentiation (especially Notch and Shh) affects the function of $Pax7^+$- MuSCs by performing a whole-mount immunofluorescence analysis in both WT and *sapje* homozygotes at 2 and 5 dpf (Fig. 9). The localization of $Pax7^+$-MuSCs in WT zebrafish was observed in niches around muscle fibers and at the myotome.[52] In *sapje* homozygotes, we observed a significant increase in $Pax7^+$- MuSCs, mainly localized near damaged muscle fibers. Moreover, a certain degree of activated and proliferating cells that incorrectly fuse to each other is also present at 5 dpf (Fig. 9B).

Notably, the increase in $Pax7^+$ MuSCs occurs in the context of a reduced Notch signaling activity, as revealed by our biosensor analysis (Fig. 6). Given the well-established role of Notch in maintaining MuSC quiescence, and regulating asymmetric division[53], its downregulation likely promotes premature activation and expansion of the $Pax7^+$ pool, while impairing proper differentiation and fusion.[54] This interpretation is consistent with the observed presence of proliferating cells that fail to correctly fuse, indicating defective regenerative commitment rather than effective muscle repair.

Then, we determined whether transcriptomic alterations translated into physiological deficits, by assessing both cytoplasmic and mitochondrial Ca^{2+} homeostasis (Fig. 10), cardiac function, mitochondrial activity, and motor behavior (Fig. 11).

To confirm in vivo the early dysregulation of Ca^{2+} homeostasis observed in RNAseq data from *sapje* zebrafish at 2 dpf, we first evaluated the cytosolic Ca^{2+} level by incubating both WT and *sapje* homozygotes with the Fluo-4 AM probe. We observed low Ca^{2+} levels in WT and elevated Ca^{2+} levels in *sapje* larvae at the level of damaged muscle fibers (Fig. 10A).

To also evaluate the mitochondrial Ca^{2+} levels, we injected fertilized eggs at one-cell stage from incrosses of *sapje* heterozygotes with 150 pg (30 ng/μl) of the pCMV-Mito4x (4mt)-GCaMP6f plasmid. After birefringence selection at 2 dpf, we observed basal Ca^{2+} levels in mitochondria of WT larvae; conversely, Ca^{2+} overload was detected in fragmented mitochondria surrounding damaged muscle fibers of *sapje* homozygotes (Fig. 10B).

To further validate early mitochondrial dysfunction associated with dysregulation of Ca^{2+} homeostasis, observed in RNAseq at 2 dpf, we measured the Oxygen Consumption Rate (OCR) and mitochondrial membrane potential at 2 dpf. Both were markedly reduced in *sapje* larvae (Fig. 11B and C), confirming impaired OXPHOS and mitochondrial organization.[50]

We used DanioScope software to analyze and quantify heartbeats in WT and *sapje* zebrafish larvae at 2 and 5 dpf. This analysis revealed significantly increased heart rate in *sapje* larvae at 5 dpf (Fig. 11A), which is consistent with upregulation of cardiac contraction genes identified by RNA-seq, and reminiscent of ventricular arrhythmias reported in pediatric DMD patients.[55,56] At this stage, heart morphology remained normal, indicating that rhythm defects precede dilated cardiomyopathy, consistent with clinical disease progression.[57]

Motor behavior was analyzed by measuring both the touch-evoked escape response at 2 dpf (Fig. 11D), and the distance moved by zebrafish larvae at 5 dpf under cycles of light/dark stimuli (Fig. 11E). Both assays revealed a significant impairment of motor behavior in *sapje* larvae, showing a lower capacity to escape after a tail-touch with a little tip (Fig. 11D), and a shorter distance moved (Fig. 11E).

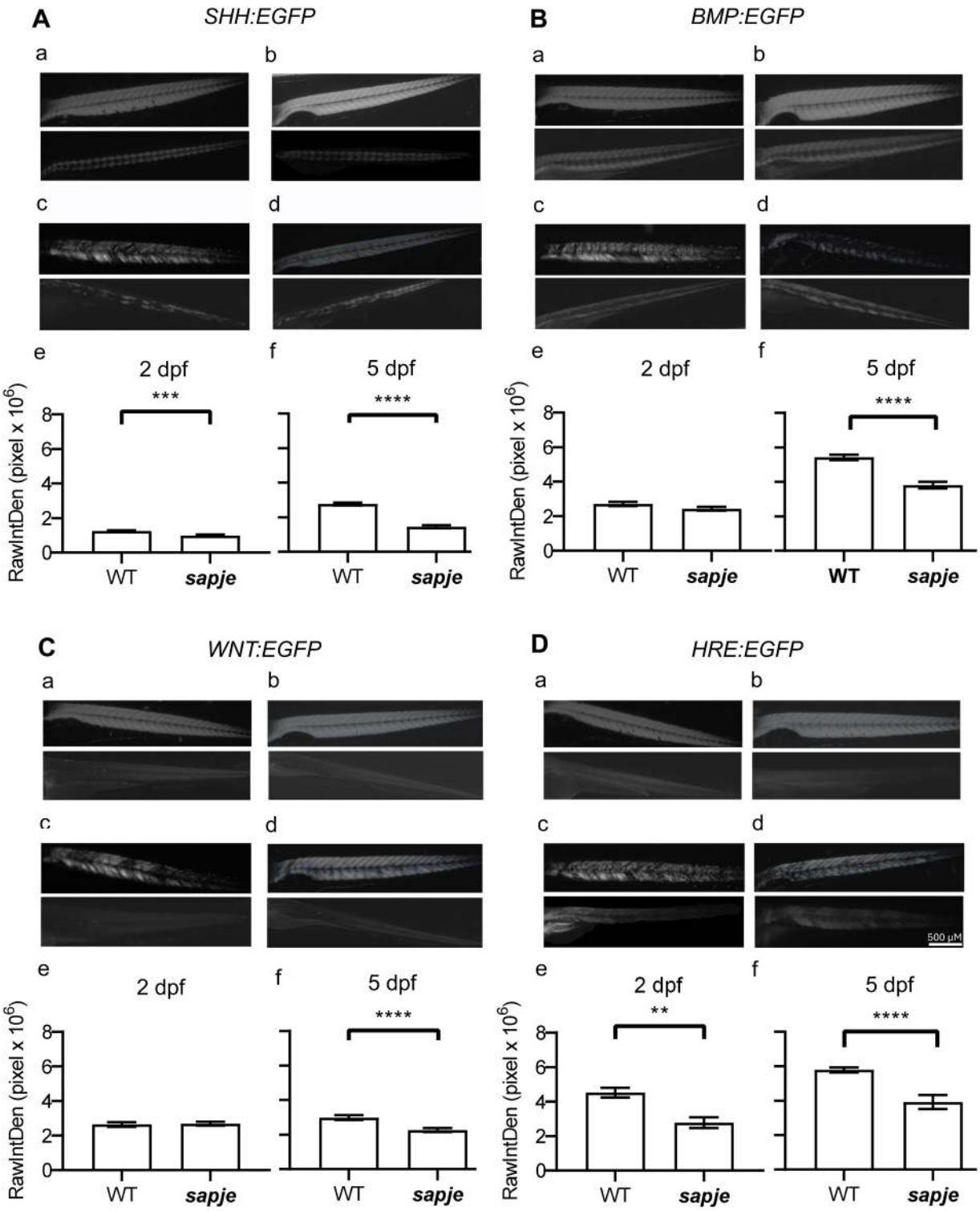

Fig. 5. Quantitative *In vivo* imaging of *sapje* biosensors. *In vivo* imaging of the *sapje;tg(4xGli1RE:eGFP)* biosensor (SHH:EGFP), *sapje:tg(4xId1RE:eGFP)* biosensor (BMP:EGFP), *sapje;tg(7xTCFl2:eGFP)* biosensor (WNT:EGFP), and *sapje;tg(4xHif-1αRE:eGFP)* biosensor (HRE:EGFP) are reported in the sections **A, B, C, and D**, respectively. All sections **(A, B, C, and D)** are organized as follows: letters **a** and **b** report the representative birefringence (upper panels) and fluorescence (lower panels) images of respectively WT embryos at 2 dpf and WT larvae 5 dpf; letters **c** and **d** report the representative birefringence (upper panels), and fluorescence (lower panels) images of respectively *sapje* embryos at 2 dpf and *sapje* larvae at 5 dpf; bar graphs in **e** and **f** represent the quantification of EGFP fluorescence signal reported as mean of raw integrated density (number of fluorescent pixels) ± s.e.m. Error bars are reported. Scale bar (white bar in section **D**) is identical for all pictures and its value is 500 µm. Number of analyzed samples: **Section A**. A total of 53 WT and 40 *sapje* were analyzed at 2 dpf; a total of 63 WT and 39 *sapje* were analyzed at 5 dpf. **Section B**. A total of 75 WT and 74 *sapje* were analyzed at 2 dpf; a total of 60 WT and 46 *sapje* were evaluated at 5 dpf. **Section C**. A total of 35 WT and 43 *sapje* were analyzed at 2 dpf; a total of 31 WT and 38 *sapje* were analyzed at 5 dpf. **Section D**. A total of 37 WT and 31 *sapje* embryos were analyzed at 2 dpf; a total of 54 WT and 31 *sapje* were analyzed at 5 dpf. ** $p < 0.01$, *** $p < 0.001$, **** $p < 0.0001$ according to Mann-Whitney unpaired non-parametric statistical analysis.

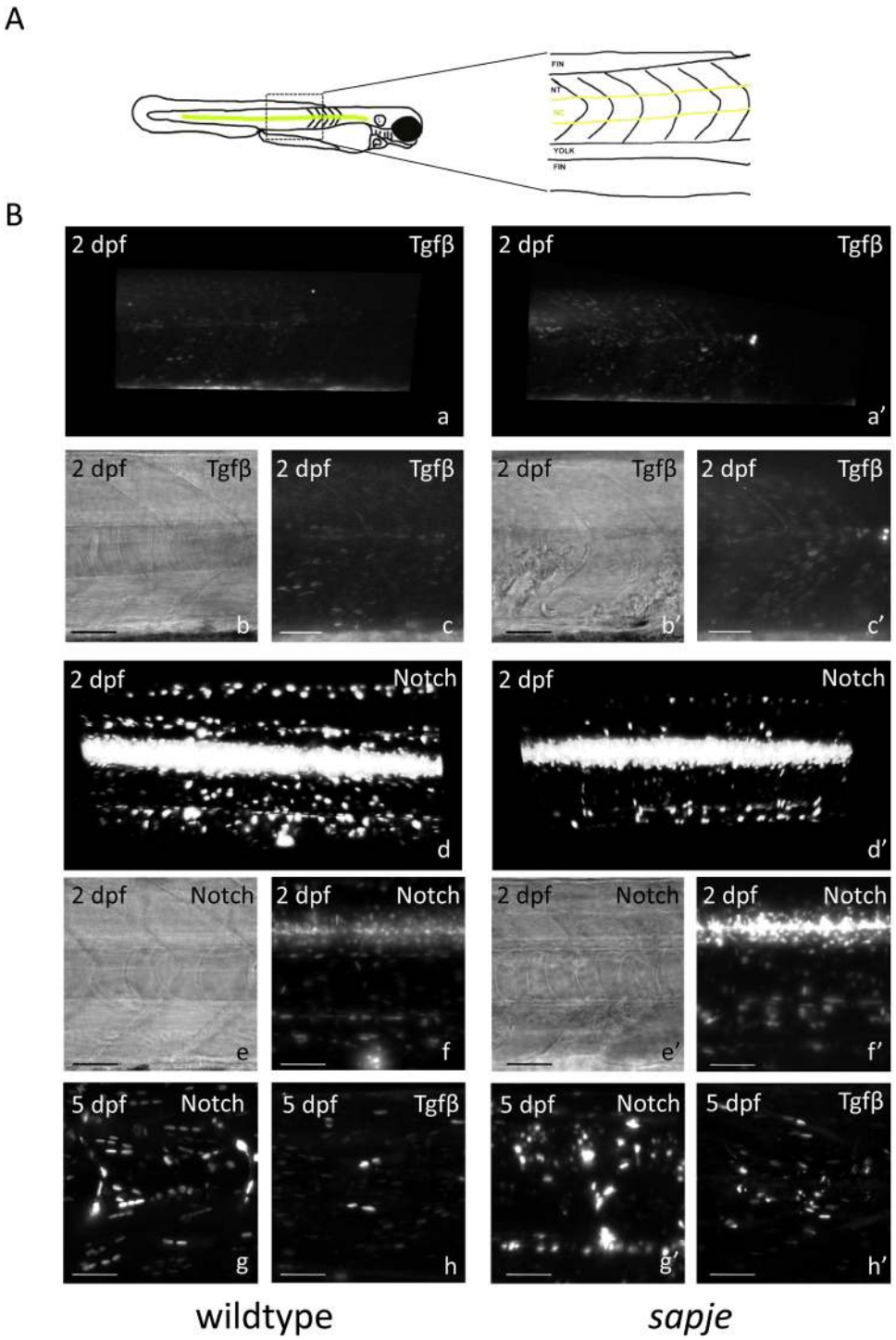

Fig. 6. Qualitative *in vivo* analysis of Tgfβ and Notch signaling pathways in WT-like and *sapje* zebrafish larvae at 2 and 5 dpf. A) Graphical schematic representation of the trunk skeletal muscle region analyzed. B) Representative lightsheet images of WT-like (a-h) and *sapje* (a'-h') larvae biosensors for Tgfβ pathway (a-c, h, a'-c', h'), and Notch pathway (d-g, d'-g'). For Tgfβ and Notch WT and *sapje* biosensors, mCherry is expressed under the control of promoter regions recognized by Smad3 Tgfβ effector and RBP-jk Notch effector, respectively. (a, a', d, d') fluorescent 3D reconstructions of the trunk region obtained with Arivis software, 0.66x magnification. (b, b', e, e') brightfield single plane image and fluorescent Maximum Intensity Projection of selected z-stacks planes (c, f-h, c', f'- h') of the above-mentioned trunk region, 1.2x magnification. Scale bar 50 μm. The experiment was repeated three times for each compound condition.

Discussion

DMD remains an incurable disorder, and despite the well-defined primary defect (the absence of dystrophin due to mutations in the *DMD* gene), mechanisms linking this defect to progressive muscle degeneration are incompletely understood.[58–61] Two main hypotheses have been proposed. The first states that the lack of dystrophin compromises sarcolemma stability, causing i) Ca^{2+} influx through microtears and Ca^{2+}-leak channels activated by excessive muscle stretching, ii) oxidative stress, and iii) mitochondrial dysfunction, ultimately leading to muscle fiber death.[13,14,62] The second hypothesis considers dystrophin and the DAPC as central components of a signal-transduction

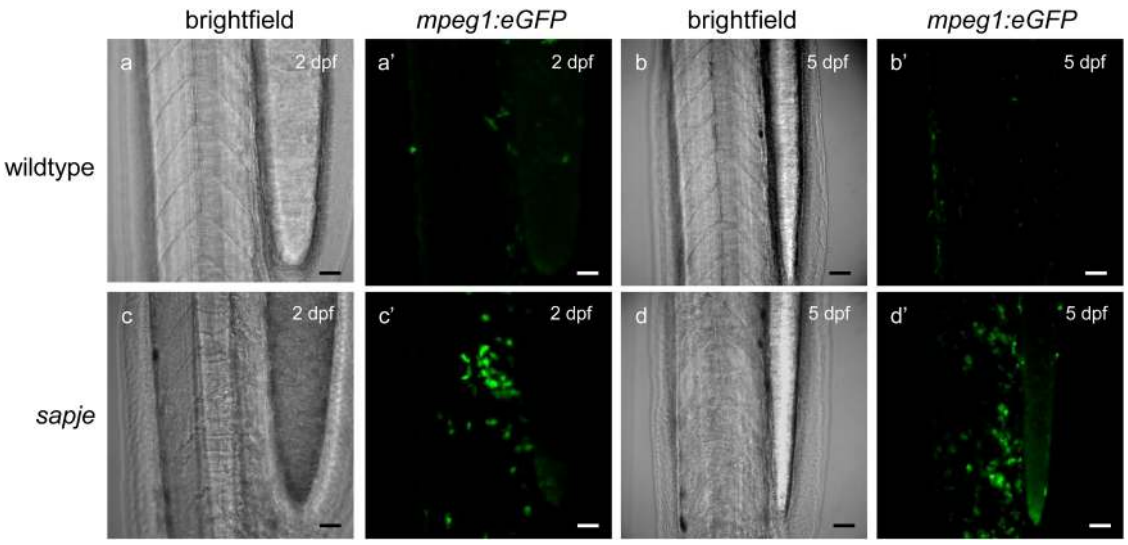

Fig. 7. Qualitative *in vivo* analysis of macrophages infiltration in *sapje* zebrafish larvae at 2 dpf and 5 dpf. Representative lightsheet images of WT and *sapje* biosensors for macrophages, expressing eGFP reporter under the control of the macrophage specific promoter *mpeg1*, at 2 (a, a', c, c') and 5 dpf (b, b', d, d'). Brightfield (a-d) and fluorescent Maximum Intensity Projection (a'-d') of selected z-stack planes of the trunk region, 0.66x magnification, are reported. Scale bar 50 μm. The experiment was repeated three times for each compound condition.

hub in both quiescent muscle satellite cells (MuSCs) and mature muscle fibers. In this model, loss of dystrophin disrupts DAPC integrity, alters the sarcolemma-ECM interface, and sensitizes quiescent MuSCs to aberrant activation and proliferation.[18] The following dysregulation of key pathways, including Ca^{2+} and Notch signaling, compromises Ca^{2+} homeostasis in both MuSCs and differentiated fibers, triggering mitochondrial dysfunction, increased glycolysis, and premature MuSCs activation. Hyperactivated MuSCs lose self-renewal capacity, becoming completely committed to regeneration. Consequently, the pool of quiescent MuSCs within the niches is progressively exhausted, and the ability of the muscle to self-regenerate is lost.[18,63] Hyperproliferating myoblasts with latent mitochondrial defects[64,65] fuse abnormally, generating hyperbranched fibers with exacerbated mitochondrial dysfunction that contribute to muscle weakness.[66,67] While both models are supported by experimental evidence, the temporal sequence and integration of these events remain poorly defined.

Our study addresses this gap by combining longitudinal transcriptomic profiling in the *sapje* zebrafish model with human DMD cell data and functional in vivo analyses, enabling reconstruction of early disease progression across multiple biological layers. Previous studies in human patients and animal models, including mouse, dog, and zebrafish, have provided important insights into the temporal progression of DMD, highlighting early inflammatory responses, metabolic alterations, and progressive muscle degeneration. However, these studies have primarily relied on transcriptomic or histological analyses at discrete time points.[68–72] Our approach provides a dynamic view of disease evolution, allowing us to identify early molecular perturbations that precede massive tissue degeneration and to link them to downstream functional consequences.

Our RNA-seq datasets from *sapje* zebrafish model and human DMD cells confirmed previous findings, identifying DEGs involved in the regulation of Ca^{2+} homeostasis, muscle development, mitochondrial function, ECM remodeling, proteasomal degradation, and metabolism.[68,70,71] Importantly, the *sapje* zebrafish model allowed us to resolve the temporal progression of these events, which is not possible in patient-derived cell lines that reflect heterogeneous mutations and later disease stages. At 2 dpf, we identified DEGs predominantly involved in the regulation of Ca^{2+} homeostasis and muscle contraction, thereby confirming the early disruption of the dystrophin-DAPC signaling transduction hub.[14,18] At 5 dpf, pathways associated with muscle repair and regeneration, ECM remodeling, cardiac involvement, and metabolic compensation were strongly upregulated. These findings support the hypothesis that hyperactivated MuSCs are fully committed to regeneration and probably fail to self-renew.[73,74] The pronounced increase in ECM deposition suggests early activation of fibrotic process driven in part by pro-regenerative M2 macrophages secreting TGFβ, a key factor promoting the activation of fibro-adipogenic progenitors (FAPs) toward adipogenesis.[75,76] The transcriptomic profile of 5 dpf *sapje* zebrafish seems to reflect both the peak of compensatory responses and the onset of accelerated disease progression. At 8 dpf, a developmental stage corresponding to advanced disease in *sapje* zebrafish, the transcriptional landscape shifts dramatically. We observed widespread downregulation of pathways essential for cell cycle progression, DNA replication, protein degradation, cell metabolism, and cell communication, indicating failure of compensatory mechanisms, and onset of irreversible muscle degeneration.[70,77] Inflammatory pathways were increasingly upregulated at this stage, consistent with chronic, unresolved damage. These findings were further supported by enrichment analyses of RNA-seq data focusing on transcription factor target genes. At 2 dpf, Pax3 target genes, which are key regulators of satellite cells self-renewal, migration, and myogenic differentiation, were already downregulated.[78,79] Mef2a and Srf target genes, which play a central role in Ca^{2+} homeostasis and myofiber maturation[40] were similarly suppressed. Notably, Pax3 target genes remained downregulated throughout disease progression, while Mef2/Srf target genes shifted substantially at later stages.

Together, these data support a model in which early Ca^{2+} dysregulation triggers mitochondrial dysfunction in both mature muscle fibers and MuSCs. Hyperactivation of MuSCs leads to loss of asymmetric division with possible impairments both in self-renewal and muscle regeneration.

While RNAseq data from *sapje* zebrafish (harboring a specific A-to-T transversion in exon 4 of the *dmd* gene, which is responsible for the complete absence of dystrophin) [22] have been useful to capture the systemic and temporal progression of the disease in a living organism, those derived from DMD patient myoblasts and myotubes (harboring different mutations in the *DMD* gene and collected at advanced stages of disease) [50] offered a focused view of intrinsic cellular defects in myoblasts and myotubes, but cannot reveal organism-level responses.[80,81] The transcriptomic data from human cell lines suggest that dystrophin deficiency affects muscle cells from early precursor stages. Human DMD myoblasts showed impaired proliferation and genomic instability, and upon differentiation, myotubes exhibited severe defects in contraction,

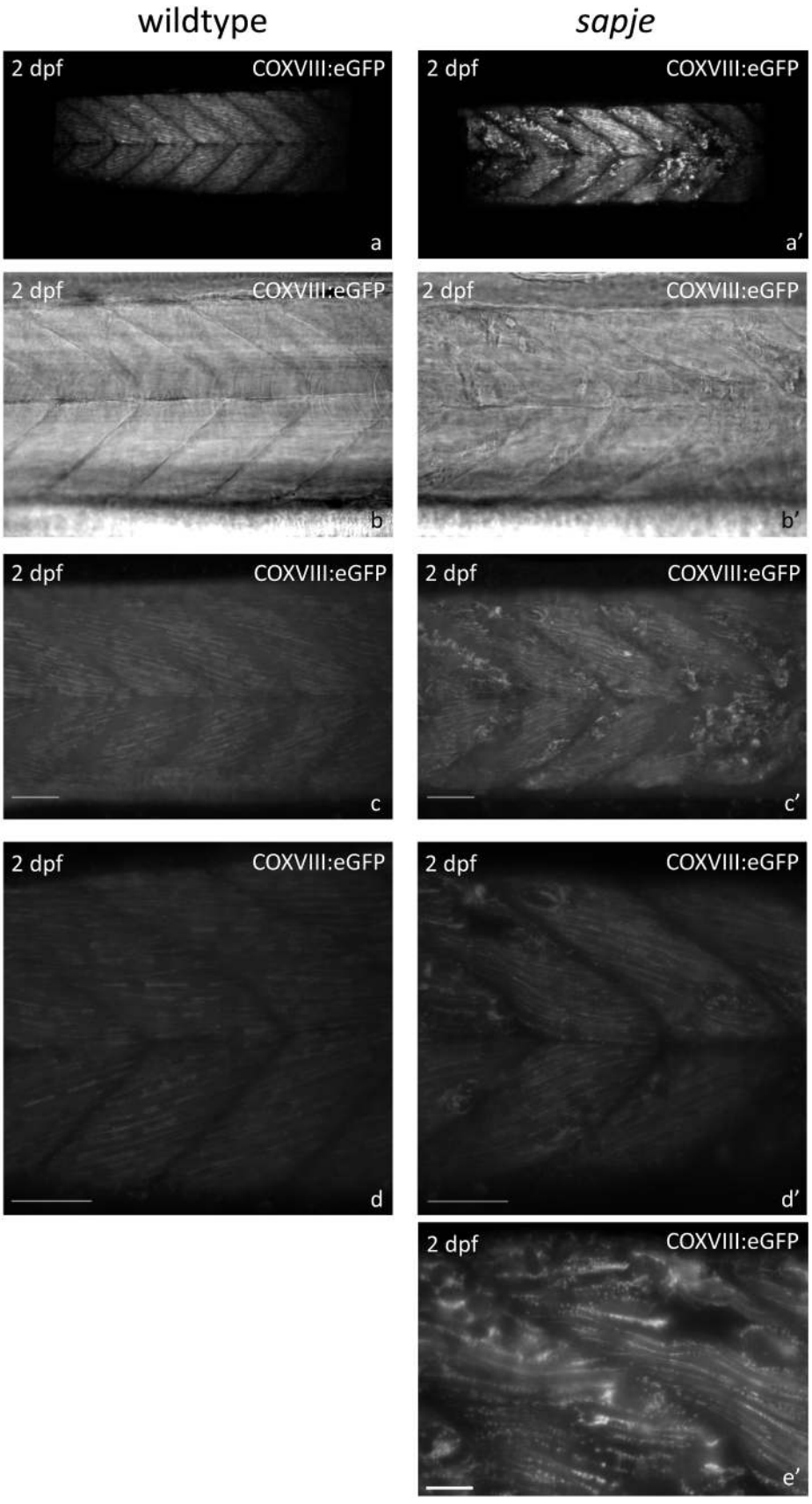

(caption on next page)

Fig. 8. *In vivo* analysis of mitochondrial activity in WT and *sapje* zebrafish larvae at 2 dpf. Representative lightsheet images of WT-like (a-d) and *sapje* (a'-e') biosensor larvae, in which GFP is expressed under a mitochondrial localization sequence (subunit VIII of cytochrome c oxygenase–COX). (a, a') fluorescent 3D reconstructions of the trunk skeletal muscle region obtained with Arivis software. (b, b') brightfield single plane image. (c, d, c', d', e') Fluorescent Maximum Intensity Projection of selected z-stack planes. (a-c, a'-c') 0.66x magnification. (d, d') 1.2x magnification, scale bar 50 μm. (e') 2x magnification, scale bar 20 μm. The experiment was repeated three times for each compound condition.

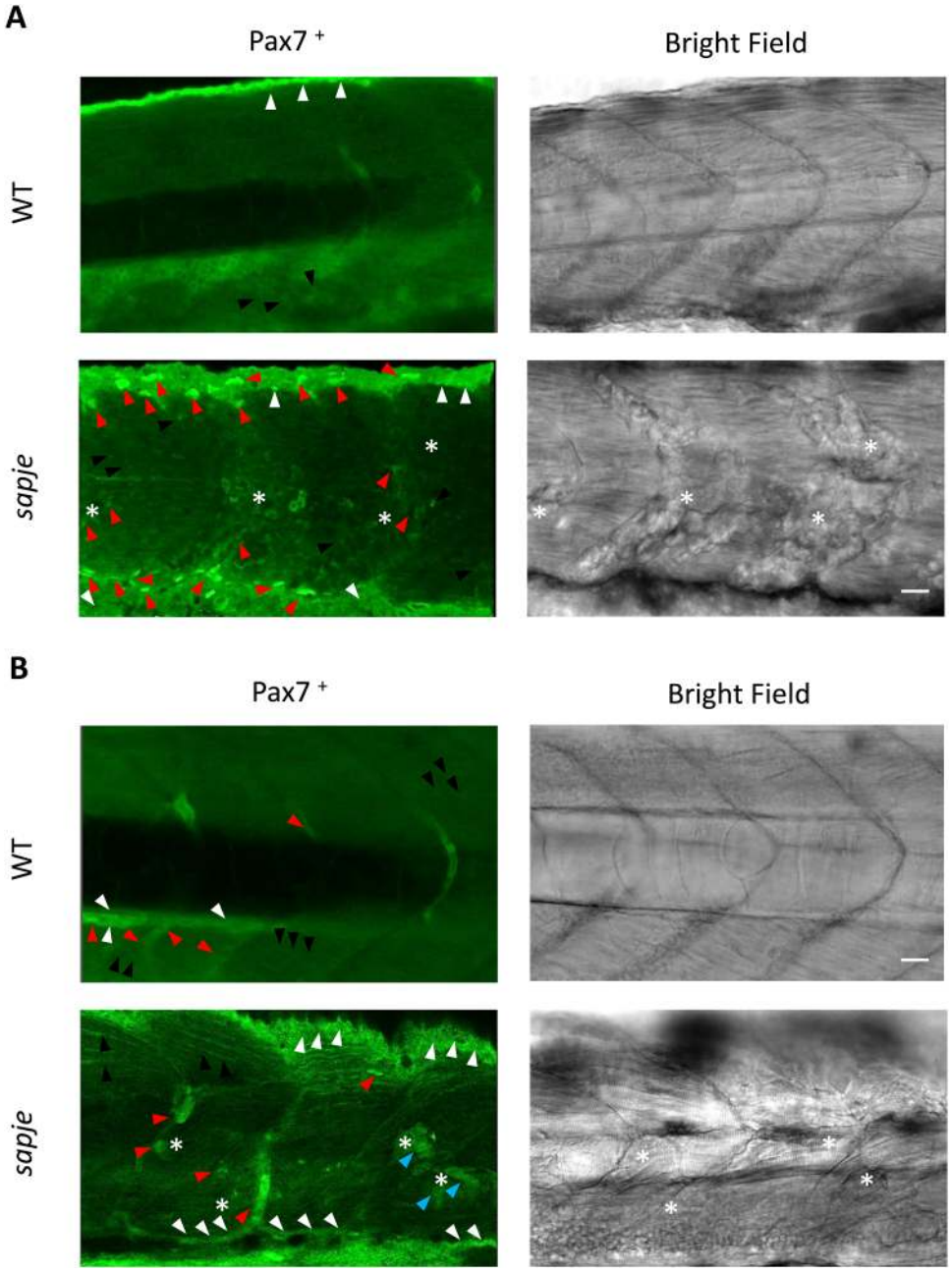

Fig. 9. Immunofluorescence of Pax7^{+}-cells. Whole-mount immunofluorescence analysis was performed at 2 and 5 dpf in wildtype (WT) and *sapje* larvae to detect Pax7^{+}-cells. (A) Representative single-plane images of WT (upper panels) and *sapje* larvae (lower panels) trunk region at 2 dpf. Representative images of Pax7 immunofluorescence (left panels) and correspondent bright filed (right panels) are reported. (B) Representative single-plane images of WT (upper panels) and *sapje* larvae (lower panels) trunk region at 5 dpf. Representative images of Pax7 immunofluorescence (left panels) and correspondent bright filed (right panels) are reported. Scale bar in A and B, 40 μM. For each analysed condition, at least 3 single planes of 3 different areas of the trunk from 3 animals were acquired. The experiment was repeated three times. Activated and proliferating Pax7^{+}-cells (red arrowheads), small Pax7^{+}-cells around muscle fibers (black arrowheads), small Pax7^{+}-cells located at the myotome (white arrowheads), alterated fusion of Pax7^{+}-cells (blue arrowheads) are indicated. White asterisks indicate regions of pronounced muscle damage.

mitochondrial energy production, and metabolism, with no evidence of compensatory responses. Notably, because myoblasts normally express little or no full-length dystrophin, their transcriptional abnormalities likely reflect alterations in the niche environment and dysregulated signaling rather than direct structural loss of dystrophin. This interpretation aligns with the model of MuSCs hyperactivation and defective

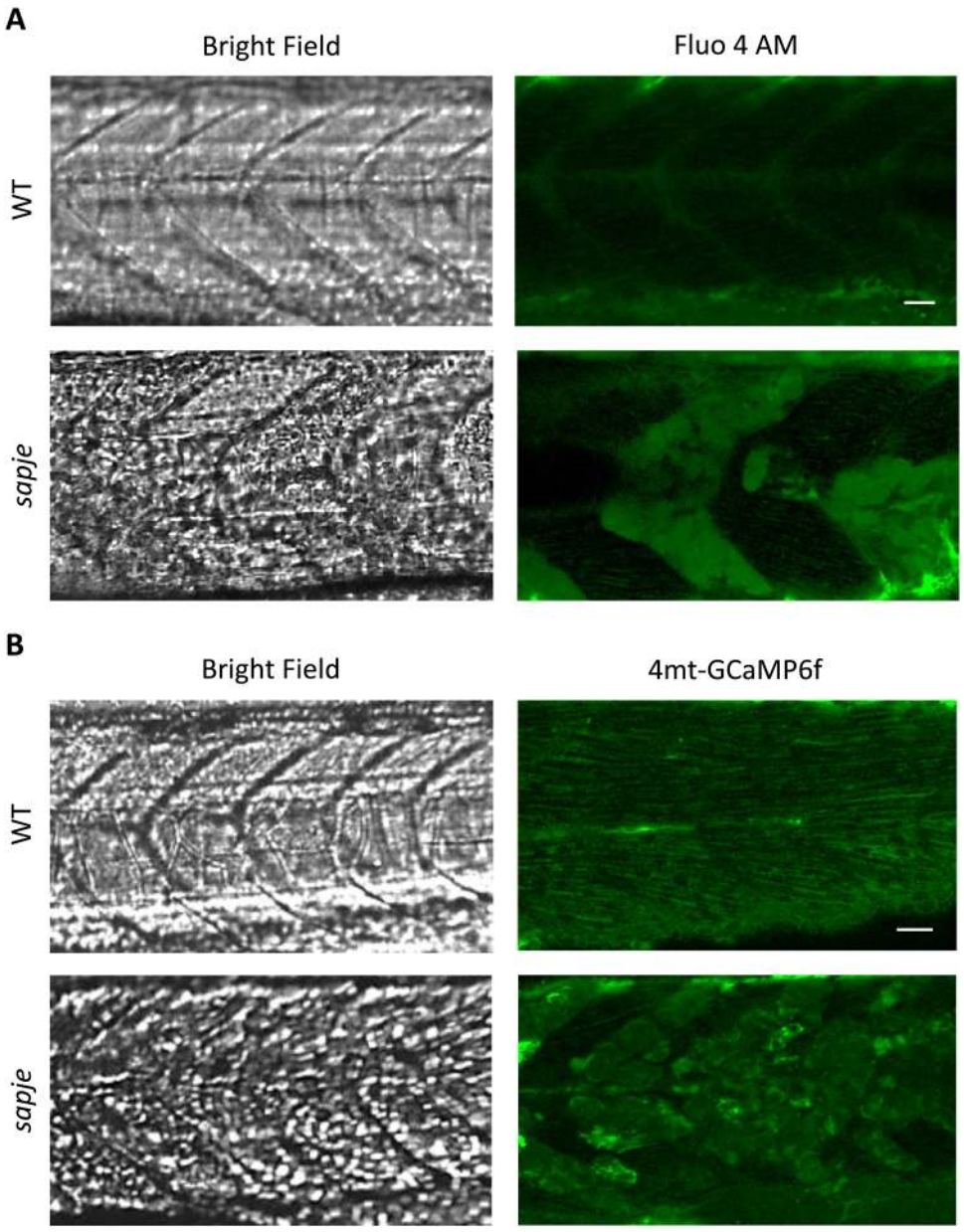

Fig. 10. Ca^{2+} imaging in living WT and *sapje* zebrafish at 2 dpf. (A) Cytoplasmic Ca^{2+} imaging of 2 dpf-old WT and *sapje* zebrafish incubated for 1 hour with 4-fluo AM probe. (B) Mitochondrial Ca^{2+} imaging of WT and *sapje* zebrafish injected at one-cell stage with a pCMV-4mtGCaMP6f plasmid containing the cDNA sequence of the 4mtGCaMP6f mitochondrial Ca^{2+} probe. All panels in A and B represent single-plane images of zebrafish trunk muscles at 2 dpf: bright filed pictures (left panels), and probe fluorescence (right panels). For each analysed condition, at least 3 single planes of 3 different areas of the trunk from 3 animals were acquired; the experiment was repeated three times. Scale bar, 50 μm.

myoblast fusion.[73,82] Overall, these findings point to early disruptions in signaling and epigenetic regulation.[73,83]

Despite deep differences between the human cell models and the *sapje* zebrafish, both systems converge on key pathological mechanisms: progressive loss of muscle function, mitochondrial dysfunction, and early activation of fibrotic process.

Mitochondrial dysfunction due to dysregulation of Ca^{2+}-homeostasis emerged as central shared hallmark. In human dystrophic myotubes, oxidative phosphorylation and mitochondrial translation were markedly downregulated. In *sapje* zebrafish, we observed a temporal sequence: early dysregulation of Ca^{2+} homeostasis (2 dpf) is followed by transient compensatory upregulation of ATP synthesis and electron transport (5 dpf), and, at advanced stages, by the almost complete collapse of mitochondrial organization and gene expression (8 dpf). While alterations in mitochondrial function, locomotion, and cardiac activity have been reported in dystrophic models, our study uniquely links these phenotypes to early transcriptomic and signaling alterations, providing a temporal framework that connects molecular defects to physiological outcomes. The presence of increased Ca^{2+} levels, as well as altered mitochondrial dynamics and functions were also confirmed by functional assays revealing (i) an increased mass of fragmented mitochondria, accumulating high Ca^{2+} levels inside, at the level of lesioned muscle fibers, suggesting DRP1-mediated fragmentation and alteration of the mitochondrial permeability transition pore (mPTP) flickering[71]; (ii) low oxygen consumption rate and mitochondrial membrane potential, probably due to the long-lasting opening of the mPTP as previously observed.[50,84] These findings point to a progressive, worsening energy crisis across models.[85,86]

Impaired regenerative capacity was another strong point of convergence between the two models. Human myoblasts showed profound

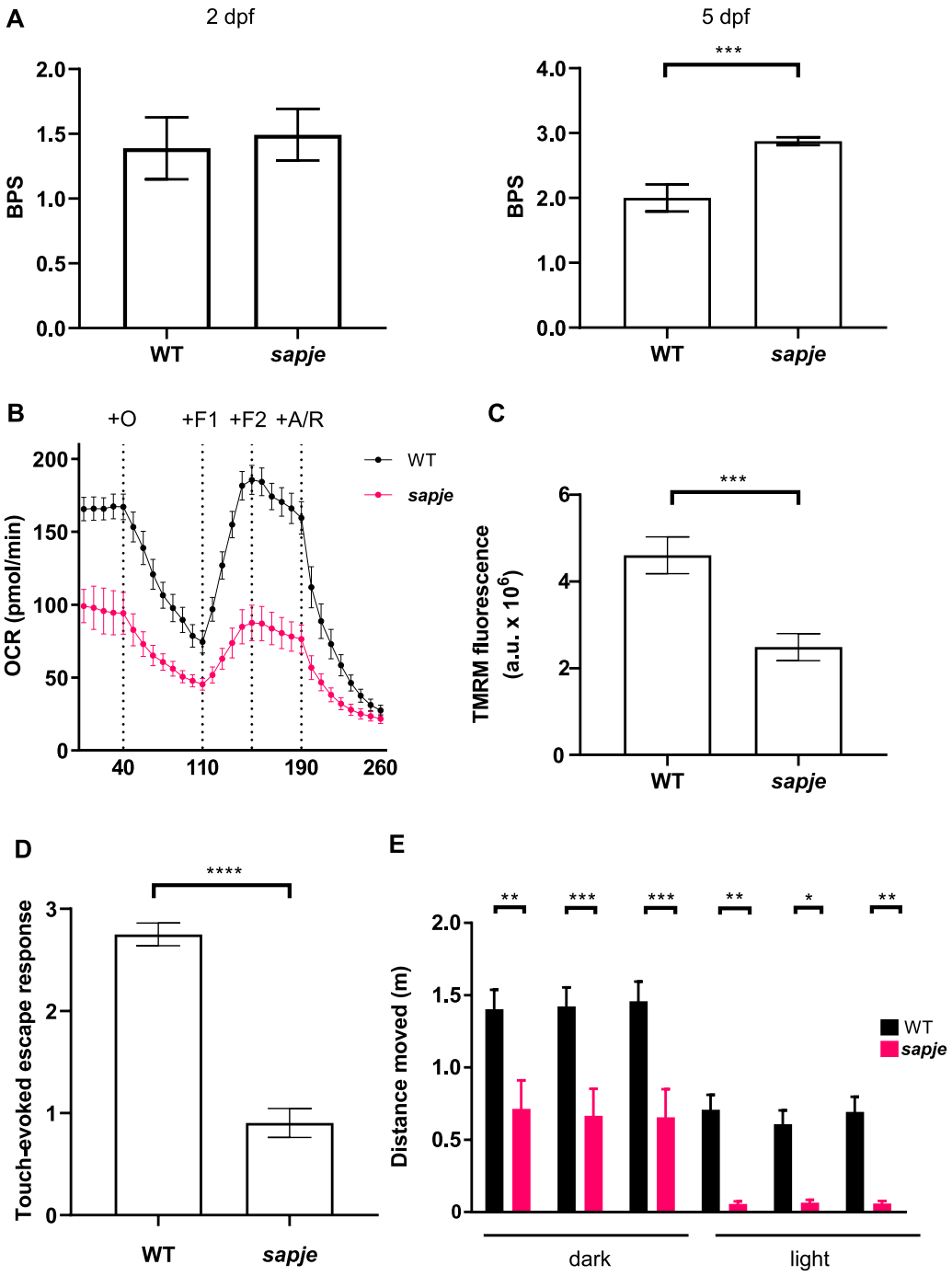

Fig. 11. Functional analyses validate RNA seq and *in vivo* imaging results. (A) Bar graphs panels represent the heartbeats per second (BPS) recorded in larvae at 2 dpf on the left (50 WT and 46 *sapje*) and 5 dpf on the right (31 WT and 30 *sapje*), respectively. Results are reported as BPS mean ± s.e.m. *p ≤ 0.05, **p < 0.01, ****p < 0.0001 according to Mann-Whitney unpaired non-parametric statistical analysis. (**B**) OCR has been measured by using XF24 Seahorse Flux Analyzer (Agilent) on 17 WT (black line) and 14 *sapje* (pink line) zebrafish larvae at 2 dpf. Results are reported as Oxygen picomoles consumed in a minute (pmol/min). Error bars for each measurement are reported. (**C**) The bar graph represents the measurement of mitochondrial membrane potential in terms of TMRM incorporation in zebrafish larvae at 2 dpf. Results are reported as a means of TMRM fluorescence pixel intensity observed in single muscle fibers ± s.e.m. *p ≤ 0.05, **p < 0.01, ****p < 0.0001, according to Mann-Whitney unpaired non-parametric statistical analysis. The experiment was carried out on 18 WT fibers and 17 *sapje* muscle fibers. (**D**) Bar graph represents the analysis of the touch-evoked escape response performed at 5 dpf on 50 WT and 22 *sapje* larvae. According to the ability of larvae to move, specific scores were assigned: 3 indicates normal movement; 2 indicates low movement; 1 indicates only the presence of spontaneous coiling events; 0 indicates complete paralysis. Results are reported as touch-evoked escape response score mean ± s.e.m. *p ≤ 0.05, **p < 0.01, ****p < 0.0001 according to Mann-Whitney unpaired non-parametric statistical analysis. (**E**) The bar graph represents the locomotor activity of *sapje* mutants (pink bars, n = 26) and WT (black bars, n = 46) at 5 days post-fertilization under three cycles of dark/light stimuli. Results are reported as the mean of the total distance moved by zebrafish larvae in each of three cycles of dark/light stimuli ± s.e.m. *p ≤ 0.05, **p < 0.01, ****p < 0.0001 according to two-way ANOVA with Bonferroni correction. All experiments in A-E were repeated in triplicate.

downregulation of pathways involved in cell-cycle progression, DNA replication, and genome maintenance, a signature that re-emerged in zebrafish at 8 dpf. This cross-species signature indicates a conserved failure of the muscle to regenerate effectively.

As mentioned before, we integrated transcriptomic profiling with in vivo biosensor imaging, which represents a major strength and innovative aspect of this study. While RNA sequencing provides a comprehensive overview of gene expression changes, it does not capture the dynamic activity of signaling pathways at the functional level. By contrast, our biosensor approach enables real-time monitoring of pathway activation in intact living organisms, revealing early signaling alterations that may not be inferred solely from transcriptional data.

Live imaging of *sapje* biosensors functionally validated and extended our transcriptomic findings by revealing early and sustained reductions in the activity of Bmp, Shh, and Notch and Hif-1α signaling pathways, which are required for satellite cell quiescence and self-renewal.[48,87–89] The persistent suppression of Notch and Hif-1α signaling pathways is consistent with the chronic upregulation of Myogenin observed in *sapje* zebrafish, indicating hyperactivation of MuSCs, and defects in asymmetric division.[47,48,68]

In addition to its role in regulating satellite cell function, Hif-1α is a key mediator of cellular responses to hypoxia and ischemia. In DMD, progressive vascular dysfunction and reduced perfusion contribute to muscle ischemia, particularly at later stages of disease.[90–93] The observed reduction in Hif-1α signaling may reflect an early defect in hypoxia sensing or metabolic adaptation. Impaired Hif-1α activity could compromise angiogenic signaling and the ability of muscle fibers to adapt to energetic stress, thereby amplifying mitochondrial dysfunction and accelerating disease progression.

Another key finding of our study is the concurrent reduction in Notch signaling activity and increase in $Pax7^+$ MuSCs, which provides mechanistic insight into early regenerative defects in DMD. Notch signaling is essential for maintaining MuSCs quiescence and regulating the balance between self-renewal and differentiation. Its suppression has been shown to induce premature activation and expansion of MuSCs, and to impair their homing during regeneration process, often at the expense of proper differentiation.[53,54]

In *sapje* zebrafish, the observed accumulation of $Pax7^+$ cells, together with their aberrant localization and defective fusion behavior, suggests that MuSCs are hyperactivated but functionally impaired. Rather than contributing to efficient regeneration, these cells likely represent a dysregulated pool that fails to restore muscle integrity. This interpretation aligns with previous findings in dystrophic models, including canine DMD, where reduced Notch signaling is associated with defective muscle regeneration.[94]

Together, these data support a model in which early Notch pathway suppression drives pathological MuSCs activation, contributing to the progressive failure of muscle repair in DMD.[90–93] Conversely, the increase in TGFβ signaling activity supports the robust fibrotic response observed by RNA-seq, identifying TGFβ as a key driver of pathological tissue remodeling.

To our knowledge, this represents one of the first studies to combine longitudinal transcriptomics with live imaging of multiple signaling pathways in a DMD vertebrate model, providing a dynamic and mechanistic framework for understanding disease initiation and progression. This platform may also be highly valuable for in vivo screening of pathway-targeted therapeutic strategies.

Collectively, our data strongly support a model in which DMD pathogenesis is initiated by Ca^{2+} dysregulation, leading to mitochondrial dysfunction, aberrant activation of MuSCs, impaired regeneration, and progressive fibrotic remodeling. From a translational perspective, our findings identify early dysregulation of Ca^{2+} homeostasis, mitochondrial function, and key signaling pathways as potential therapeutic targets. Interventions aimed at preserving mitochondrial integrity or restoring signaling pathways such as Notch or Hif-1α may be particularly effective if applied at early disease stages, before irreversible muscle degeneration occurs. The cross-species convergence observed between zebrafish and human models further supports the clinical relevance of these targets.

Materials and methods

Zebrafish maintenance

WT Zebrafish (AB strain), *sapje* heterozygous mutants, and the previously generated transgenic reporter lines[43] kindly provided by the Zebrafish Facility at the University of Padova, have been maintained according to standard protocols[95] with a 14-10 light-dark cycle at 28.5°C, in aerated saline water, at the Zebrafish Facility of the University of Brescia. Male and female animals have been separated in the late afternoon to allow, the next morning, courtship, egg deposition, and fertilization.

Embryos have been collected in Petri dishes and maintained at 28.5°C in fish water (3 mg/l Instant Ocean, 0.5 mM NaHPO4, 0.2 mg/l methylene blue, 0.5 mM NaH2PO4). All animal procedures on zebrafish larvae older than 5 dpf have been performed in compliance with the European Directive 2010/63/EU, all the Animal Care Standard Operating Procedures (ARRIVE guidelines 2.0), and and the Guidelines for the Care and Use of Laboratory Animals issued by the Italian Ministry of Health. The study has been approved by the Italian Ministry of Health (Authorization n. 60/2023).

Cells

Immortalized myoblast cell lines from two DMD patients and one healthy donor (Supplementary Table 13), generated at the Institute of Myology (Pitié-Salpétrière Hospital, Paris, France), as described in[50] by double transduction of primary myoblasts with hTERT and cdk4, have been kindly provided by Prof. Vincent Mouly, Institute of Myology, Sorbonne University, Paris.[50,96]

Immortalized myoblast cell lines were expanded in proliferation medium (Skeletal Muscle Cell Growth medium, PromoCell C-23060), supplemented with penicillin and streptomycin. For differentiation, myotubes were obtained by exposing confluent myoblast cultures to Skeletal Muscle Cell Basal medium (PromoCell C-23260), supplemented with insulin 10 μg/mL (Sigma), penicillin, and streptomycin for 7 days. Cell media were changed every 2-3 days in culture.

Primary myoblasts obtained from muscle biopsies of 1 DMD patient and two healthy donors (Supplementary Table 13) have been kindly provided by Orthopedic Institute Rizzoli in Bologna, Bologna, Italy, following ethics committee approval and informed consents. Cultures were prepared by enzymatic and mechanical treatment of muscle biopsies and by plating in Dulbecco's modified Eagle's medium (DMEM) supplemented with 20% fetal calf serum, penicillin, streptomycin, and amphotericin B (Sigma) as previously described [97] and stored in liquid nitrogen. Cells were expanded and used within the 7th passage.[98] The study was conducted in accordance with the Declaration of Helsinki, and the protocol was approved by the Ethics Committee at the Rizzoli Orthopedic Institute (project identification code: CE 0007151, 11 May 2021).

RNA sequencing

Total RNA from zebrafish embryos and human cell lines was isolated with the kit Quick DNA/RNA MiniPrep Plus (ZYMO Research D7003) and quantified with a nanodrop. A total of 22 embryo pools (approximately 45 embryos per pool) from WT and *sapje* mutants at 2, 5, and 8 dpf were analyzed. Details are reported in Supplementary Table 14.

Prior to library preparation, sequin (synthetic RNA spike-in controls) were added to the mRNA as sequencing internal controls.[99] The spike-in analysis revealed a gene detection sensitivity of 0.059 attomol/μl. The correlation between the input concentration and the measured

concentration of the sequins was 0.91 ± 0.04 in zebrafish and 0.92 ± 0.17 in human samples; r2 of the linear model was 0.83 ± 0.08 in zebrafish and 0.75 ± 0.18 in human samples. The high correlation indicates excellent recovery of the spike-in mix during the entire library preparation and sequencing workflow. Libraries were produced with QuantSeq 3′ mRNA-Seq Library Prep Kit for Ion Torrent (Lexogen), according to the manufacturer's instructions and quantified with the QIAseqTM Library Quant Assay Kit (Qiagen).

For zebrafish samples, the templates were prepared with the Ion PI Hi-Q OT2 200 Kit on the Ion OneTouch 2 System and sequenced on the Ion Proton System with Ion PI Hi-Q Sequencing 200 Kit (Ion Torrent by Thermo Fisher Scientific). For human samples, the templates were prepared with the 540 Kit – OT2 kit (Ion Torrent by Thermo Fisher Scientific) on the Ion OneTouch 2 System and sequenced on the Ion S5 System.

Demultiplexing and barcode trimming were performed automatically by the Torrent Suite Software after each sequencing run. Following the guidelines of Lexogen manufacturer, we used cutadapt[100] to cut poly-A tails and five bases from the 5′ prime end (which may contain mismatched bases eventually introduced by random priming). After trimming, all reads with a length below 30 bp and quality trimming below Q10 were discarded. The quality of processed data was evaluated by analyzing the sequins spike-in transcripts using Kallisto[101] and the Anaquin package in R.[102]

For zebrafish samples, after QC, STAR aligner v. 2.6 was used to compute the reads alignment and gene counts based on the *Danio rerio* reference genome (GRcz11) and the Ensemble comprehensive gene-set annotations. After merging data from all samples, only genes with >10 reads in at least 3 samples were included, resulting in a gene count matrix with 22 samples and 19035 genes. In all three comparisons (*sapje* vs wt at 2, 5, and 8 dpf) 18966 out of 19035 genes were analyzed; 43, 5 and 23 genes were not analyzed at 2, 5 and 8 dpf, respectively, either because the total read count was zero, or because of the presence of a sample pool with an extreme count outlier in that specific comparison.

For human samples, read alignment and gene counts were based on the *Homo sapiens* reference genome (GRCh38) and the Ensemble comprehensive gene-set annotations. After combining the data from all the samples and filtering out genes that had fewer than 10 reads in fewer than 3 samples, we obtained a gene count matrix with 12 samples and 18103 genes.

Whole transcriptome analyses

Identification of Danio rerio differentially expressed genes

The gene expression analysis was performed using the DESeq2 package in R, as described in.[103] Principal Component Analysis (PCA) was performed with the PlotPCA function implemented in the DESeq2 package on the regularized log-transformed (rlog) data, using the top 15000 genes selected by highest row variance.

To identify DEGs in our *sapje* zebrafish model, we performed two distinct analyses. The first analysis aimed to identify genes whose expression significantly changed over time, specifically looking for those with different trajectories between WT-type and mutant fish. For this, we employed a design that included status (WT/dmd) as a factorial variable, time as a continuous variable, and the interaction between status and time. This allowed us to capture genes whose expression levels varied in a time-dependent manner and, critically, those where this time-dependent variation differed between WT and *sapje* zebrafish. In our secondary analysis, we performed direct comparisons of gene expression between WT and *sapje* zebrafish at each time point (2 dpf, 5 dpf, and 8 dpf). Since principal component (PC) analysis clearly showed that the expression profiles of the embryos are different at 2-, 5-, and 8-days post fertilization (dpf) (Supplementary Fig. 1A). For this reason, subsequent analyses were conducted separately on the three groups. PCA also uncovered a minor batch effect, which is attributable to the fact that the WT-like embryos are siblings of the mutant ones (Supplementary Fig. 1B). The "family effect" was removed with the Combat seq tool.[104] ComBat-seq adjusted data were then analyzed with the Wald test implemented in DESeq2 to identify differentially expressed genes (DEGs). Due to a partial collinearity between the "family effect" and the time variable, it has not been possible to apply ComBat-seq in the longitudinal analysis.

False discovery rate BH FDR was used to control for multiple test comparisons, and genes with FDR < 0.05 were considered as DEGs.

A hypergeometric test was applied to test if the number of common DEGs at the three time points was significantly higher than expected by chance.

Identification of human differentially expressed genes

The human cell line differential expression analysis was performed with the DESeq2 package as described above for the zebrafish embryos. In this case, PCA revealed a "laboratory of origin" batch effect (Supplementary Fig. 2) that was removed by the ComBat-seq tool prior to performing differential expression analysis. ComBat-seq adjusted data were analyzed with the Wald test implemented in DESeq2 separately in myoblast and myotubule cell lines to identify differentially expressed genes (DEGs).

Gene set enrichment analyses (GSEA)

Gene-set enrichment analysis was performed using WebGestaltR v. 4.0.3, and the GSEA enrichment method.[105] Enrichment categories considered were: GO Biological Process, Reactome pathways, and network Transcription Factor target. Only enrichment categories with >20 genes and <500 genes were analyzed, and those categories with FDR < 0.05 were considered significantly enriched. The EnrichmentMap Cytoscape App[106] was used to visualize the results of the enrichment process as a network.

Integrated analysis of RNA-seq data

The list of 21973 human-zebrafish pairs of orthologue genes was retrieved from Ensembl using the "getLDS" function in the biomaRt package in R. The list of orthologs was then intersected with the list of genes analyzed in this study to identify common genes in the two species.

To test if the number of orthologue genes found differentially expressed both in human and zebrafish was higher than expected by chance, we applied a random statistic test. Briefly, on the overall set of human-zebrafish pairs of orthologs addressable in our analysis (background genes), we randomly sampled N pairs, with N equal to the number of pairs of orthologue genes found differentially expressed in human, and we counted how many pairs were differentially expressed in zebrafish at 2, 5, and 8 dpf. The procedure was repeated 10 million times. Empirical p-values were then calculated as the number of tests resulting in an equal or higher number of overlapping genes than those observed in our data.

Birefringence

To isolate the 25% of *sapje* homozygotes and to assess muscle fiber structure integrity, birefringence analysis has been performed on Zebrafish embryos at 48 hpf. This assay takes advantage of muscle fiber anisotropy, which is the ability of well-organized muscle fibers to refract polarized light. Briefly, a first polarized filter is placed directly on the microscope base to polarize the white light. Secondly, the polarized light passes through the anisotropic muscle fibers that refract it. A second polarized filter controls the refraction angle. Normal muscle fibers appear with a brilliant signal, while altered muscle fibers appear dark.[107]

Generation of sapje biosensors and fluorescence analyses

To study the dynamics of both mitochondrial patterning and the

expression of different signaling pathways at different stages of DMD pathogenesis, we generated specific *sapje* biosensors, expressing fluorescent reporters, such as GFP or mCherry, under the control of a specific mitochondrial promoter or promoter-responsive elements recognized by a specific signaling pathway's effector. To generate *sapje* biosensors, adult non-fluorescent heterozygous *sapje* were outcrossed with adults of the previously generated transgenic reporter lines.[43] The obtained *sapje* biosensors for mitochondrial patterning and Notch, Tgfβ, Shh, Wnt, Bmp, Hif-1α signalling pathways were then incrossed to obtain 25% of homozygous that were further analyzed for fluorescence together with their WT-like siblings. Images of embryos and larvae from WT-like and *sapje* biosensors were acquired at 2 and 5 dpf, to obtain a relative quantification of the intensity of fluorescence with ImageJ. Concerning the mCherry reporter lines, the intensity of fluorescence was not quantifiable due to the lower rate of expression of this reporter protein compared to GFP, whose expression is really fast. Thus, qualitative images of WT-like and *sapje* homozygous mCherry biosensors were acquired by using the Zeiss lightsheet microscope. At least 3 samples for each condition in each experimental replicate have been acquired.

Behavioral assays

Two behavioral assays were carried out on WT-like and *sapje* homozygotes at 5 dpf: i) the touch-evoked escape response, which has been performed to evaluate the ability of larvae to move away after mechanical stimuli; and ii) the measurement of the distance moved after a light/dark stimulus, which has been performed using the DanioVision system coupled with EthoVision XT software (Noldus Information Technology, The Netherlands) to evaluate fish motility.

Concerning the touch-evoked escape response, fish movements were recorded, and a score was assigned to each embryo. The score goes from zero to three: i) three is associated with the WT phenotype; ii) two is assigned to a short distance moved; iii) one is linked to the spontaneous coiling events; iii) zero is assigned to paralyzed animals.

Noldus recordings were performed at 5 dpf from ZT 1 to ZT 6, in a 24-well plate with a temperature close to 28°C and a constant final volume of 0.5 mL per well. After 30 minutes of habituation in light conditions, larvae were exposed to 3 cycles composed of 10 minutes of dark and 10 minutes of light.

Seahorse

Oxygen consumption rates (OCR) were measured using the Seahorse XF-24 extracellular flux analyzer that allows the detection of oxygen consumption through a sensor cartridge, which was equilibrated in 1 ml of calibrant medium overnight at 28°C. After equilibration, OXPHOS modulators, such as oligomycin (complex V inhibitor), FCCP (uncoupling agent), Antimycin A (complex III inhibitor), and rotenone (complex I inhibitor), were added at 10 μM, 1 μM, 1 μM, and 1 μM, respectively. Wt-like and *sapje* larvae at 2 dpf were placed in 24-well islet capture Seahorse plates and the experiments were run at 28.5°C. OCR of at least 20 embryos wt-like and *sapje* homozygotes was analyzed.[50,98]

Heartbeat

Sapje and WT-like larvae heartbeats were recorded at 2 and 5 dpf with the Axiozoom V16 Zeiss stereomicroscope at 32x zoom. Acquired videos were exported at 20 fps and then analyzed with the DanioScope software to evaluate the presence of alterations.

Mitochondrial membrane potential

Mitochondrial membrane potential was evaluated by measuring the uptake of tetramethylrhodamine methyl ester (TMRM). Zebrafish embryos at 2 dpf were exposed to 300 nM TMRM supplemented with 1.6 μM CsH for 4 hours at 28.5°C. After a brief wash with embryo medium, animals were anesthetized and mounted in 1% low-melting agarose. A single plane images were acquired with the Zeiss confocal microscope to allow analysis. The experiment was repeated three times for each condition.[98]

Ca^{2+} homeostasis

Cytosolic Ca^{2+} homeostasis was evaluated with the Fluo-4 AM probe. Single zebrafish samples at 2 dpf (WT and *sapje* homozygotes preselected by birefringence) were exposed to a 1 μM final concentration of the Fluo-4 AM probe, diluted in embryo medium, for 1 hour as previously described.[108] After incubation, samples were briefly washed, anesthetized and mounted in 1% low-melting agarose. The experiment was conducted in triplicate and at least 3 single plane images of 3 different areas from at least 3 zebrafish samples per condition were acquired with Leica TCS SP5 AOBS confocal-multiphoton.

Mitochondrial Ca^{2+} levels were evaluated by injecting one-cell stage embryos from incrosses of *sapje* heterozygotes with 150 pg (5 nl of 30 ng/μl dilution) of the pCMV-Mito4x-GCaMP6f plasmid, kindly gifted by Dr. Riccardo Filadi, Senior Researcher at the CNR, University of Padua. WT and homozygote samples were selected by birefringence at 48 hpf, anesthetized and mounted in 1% low-melting agarose. As previously mentioned, at least 3 single plane images of 3 different areas from at least 3 zebrafish samples per condition were acquired with Leica TCS SP5 AOBS confocal-multiphoton.

Whole-mount immunofluorescence

Zebrafish embryos at 2 and 5 dpf, WT-like and *sapje* were fixed for 4 h in 4% PFA and washed in PBS supplemented with 0.1% Tween 20 (PBT). Embryos were then permeabilized for 30 min or 90 min, depending on dpf, with 10 μg/mL proteinase K in PBT and briefly post-fixed in 4% PFA for 15 min. 3 PBT washes of 10 min precede an RT incubation of 1% DMSO in PBT for 20 min, followed by two PBT washes. Samples were then blocked with 2% FBS, 2% BSA and 1% DMSO in PBT O.N. at +4°C. Embryos were then incubated at +4°C for 72 h with the primary monoclonal anti-Pax7 Ab produced in mouse diluted 1:100 in blocking solution. After incubation, samples were washed with PBST +1% DMSO and incubated with secondary anti-mouse Alexafluo 488-conjugated antibody diluted 1:500 in blocking solution at 4°C for 48 h. After several washes in PBT, at least 3 single plane images of 3 different areas from at least 3 zebrafish samples per condition were acquired with Evident FV4000 inverted confocal.

Statistics

The statistical analyses were performed with GraphPad Prism 8.4.2 software, except for RNA sequencing data, which were analyzed with R.

Analyses of fluorescence quantification, BPS, TMRM, and touch-evoked escape response have been performed with Mann-Whitney unpaired non-parametric test, and all relative data are reported as mean values ± standard error of the mean (SEM). The distance moved, analyzed with the Noldus DanioVision chamber, has been evaluated and quantified using Ethovision software (Noldus) and statistically analyzed with the two-way ANOVA with Bonferroni correction. In all the analyses, the statistical significance was fixed at $p \leq 0.05$.

Abbreviations

DMD	Duchenne muscular dystrophy
BMD	Becker muscular dystrophy
Ca^{2+}	Calcium ion
MuSCs	muscle satellite cells
NOS	Nitric oxide synthase
DAPC	Dystrophin-associated protein complex
ROS	Reactive oxygen species
PAX3	Paired box 3 gene

MYOG	Myogenin gene
TF	Transcription factor
FAPs	Fibro-adipogenic progenitors
dpf	Days post-fertilization
WT	Wildtype
DEGs	Differentially expressed genes
GSEA	Gene Set Enrichment Analysis
OCR	Oxygen consumption rate
TMRM	Tetramethyl-Rhodamine-Methyl ester
CsH	Cyclosporin H
PTP	Permeability transition pore
ECM	Extracellular matrix
OXPHOS	Oxidative phosphorylation
GFP	Green fluorescence protein
SHH	Sonic hedgehog gene
TGFβ	Transforming Growth Factor beta
BMP	Bone morphogenetic protein
HIF-1α	Hypoxya inducible factor – 1 alpha
WNT	Wingless-Type MMTV Integration Site Family
S.E.M.	Standard Error Mean
BPS	Heartbeats per second
MEF2	Myocyte enhancer factor 2
SRF	Serum response factor
NFATC4	Nuclear factor of activated T cells 4
ARRDC3	Arrestin domain containing 3
CADM2	Cell adhesion molecule 2
PRELP	Proline and arginine rich end leucine rich repeat gene
TCEA3	Transcription elongation factor A3
RPL23AP74	Ribosomal protein L23a pseudogene 74 gene
SCF	Stem cell factor
APC	Adenomatous Polyposis Coli
NIK	NF-kB-inducing kinase
NF-kB	Nuclear factor kappa B gene
FCERI	Fc epsilon receptor 1
MTND3P25	Mitochondrial encoded NADH:Ubiquinone Oxidoreductase Core subunit 3 pseudogene 25
ELK1	Elongation transcriptor factor kinase ELK1
ZTBTB14	Zinc finger and BTB domain containg 14
SF1	Steroidogenic factor 1
MPEG	Macrophage expressed gene

Funding

This study was supported by the AFM-Telethon (Trampoline Grant application n. 25937 titled "Identification of new druggable targets for Duchenne Muscular Dystrophy").

Data availability

The data and/or experimental protocols that support the findings of this study are available from the corresponding author upon reasonable request. Some data may not be made available because of privacy or ethical restrictions.

The RNAseq data generated and analysed during the current study are available in the NCBI's Gene Expression Omnibus repository - ID: GSE289373.

Declaration of generative AI and AI-assisted technologies in the manuscript preparation process

During the preparation of this work the authors used the basic version of ChatGPT (https://chatgpt.com) in order to improve language and readability of the manuscript. After using this tool, the authors reviewed and edited the content as needed and take full responsibility for the content of the published article.

CRediT authorship contribution statement

Elena Cannone: Writing – original draft, Validation, Methodology, Investigation, Formal analysis, Data curation. **Martina La Spina:** Writing – original draft, Methodology, Investigation. **Barbara Gnutti:** Methodology, Investigation, Formal analysis, Data curation. **Chiara Tesoriero:** Validation, Methodology, Formal analysis. **Silvia Castagnaro:** Validation, Methodology. **Chiara Tobia:** Validation, Methodology, Formal analysis, Data curation. **Luca La Via:** Methodology, Formal analysis. **Patrizia Sabatelli:** Resources, Methodology, Formal analysis. **Cesare Faldini:** Resources. **Giuseppe Fiume:** Writing – original draft, Visualization, Methodology. **Andrea Vettori:** Writing – original draft, Validation, Supervision. **Dario Finazzi:** Validation, Supervision. **Massimo Gennarelli:** Resources, Project administration. **Chiara Magri:** Writing – original draft, Validation, Supervision, Software, Investigation, Formal analysis, Data curation, Conceptualization. **Marco Schiavone:** Writing – original draft, Validation, Supervision, Project administration, Investigation, Funding acquisition, Formal analysis, Data curation, Conceptualization.

Declaration of competing interest

The authors declare no conflict of interest.

Acknowledgements

We acknowledge Prof. Paolo Bernardi for his suggestions and critical reading of the manuscript; AFM-Telethon for funding this project with the Trampoline Grant application n. 25937 titled "Identification of new druggable targets for Duchenne Muscular Dystrophy"; Vincent Mouly for immortalized patient cells; Zebrafish Facility of UNIBS at the Department of Molecular and Translational Medicine, UNIBS, for hosting mutant and transgenic lines used to conduct this work; NGS Facility at the Department of Molecular and Translational Medicine, UNIBS, for hosting all the equipment necessary to conduct RNA sequencing analysis; Laboratory of Cellular Bioenergetics at the Department of Molecular and Translational Medicine, UNIBS, for the use of Seahorse XFe24 Analyzer; Prof. Paolo Bonaldo, Department of Molecular Medicine, University of Padova, for providing us with Pax7 antibody; Dr. Riccardo Filadi, Senior Researcher at CNR, Department of Biomedical Sciences, University of Padova; CPT platform of the University of Verona for the use of Leica TCS SP5 AOBS confocal-multiphoton and the EVIDENT FV4000 Inverted confocal microscope.

Supplementary materials

Supplementary material associated with this article can be found, in the online version, at doi:10.1016/j.trsl.2026.06.007.

References

1. Hoffman EP, Brown RH, Kunkel LM. Dystrophin: the protein product of the Duchenne muscular dystrophy locus. *Cell*. 1987;51(6):919–928. https://doi.org/10.1016/0092-8674(87)90579-4.
2. Mercuri E, Bönnemann CG, Muntoni F. Muscular dystrophies. *Lancet*. 2019;394(10213):2025–2038. https://doi.org/10.1016/S0140-6736(19)32910-1.
3. Duan D, Goemans N, Takeda S, Mercuri E, Aartsma-Rus A. Duchenne muscular dystrophy. *Nat Rev Dis Primers*. 2021;7(1):13. https://doi.org/10.1038/s41572-021-00248-3.
4. Aartsma-Rus A, Ginjaar IB, Bushby K. The importance of genetic diagnosis for duchenne muscular dystrophy. *J Med Genet*. 2016;53(3):145–151. https://doi.org/10.1136/JMEDGENET-2015-103387.
5. Muntoni F, Desguerre I, Guglieri M, et al. Ataluren use in patients with nonsense mutation Duchenne muscular dystrophy: patient demographics and characteristics from the STRIDE Registry. *J Comp Eff Res*. 2019;8(14):1187–1200. https://doi.org/10.2217/CER-2019-0086/SUPPL_FILE/SUPPLEMENTARY.
6. Ervasti JM, Sonnemann KJ. Biology of the striated muscle dystrophin-glycoprotein complex. *Int Rev Cytol*. 2008;265:191–225. https://doi.org/10.1016/S0074-7696(07)65005-0.

7. Constantin B. Dystrophin complex functions as a scaffold for signalling proteins. *Biochim Biophys Acta*. 2014;1838(2):635–642. https://doi.org/10.1016/j.bbamem.2013.08.023.
8. Gao QQ, McNally EM. The dystrophin complex: structure, function, and implications for therapy. *Compr Physiol*. 2015;5(3):1223–1239. https://doi.org/10.1002/cphy.c140048.
9. Zhao J, Kodippili K, Yue Y, et al. Dystrophin contains multiple independent membrane-binding domains. *Hum Mol Genet*. 2016;25(17):3647–3653. https://doi.org/10.1093/hmg/ddw210.
10. Le S, Yu M, Hovan L, Zhao Z, Ervasti J, Yan J. Dystrophin As a molecular shock absorber. *ACS Nano*. 2018;12(12):12140–12148. https://doi.org/10.1021/acsnano.8b05721.
11. Starosta A, Konieczny P. Therapeutic aspects of cell signaling and communication in Duchenne muscular dystrophy. *Cell Mol Life Sci*. 2021;78(11):4867–4891. https://doi.org/10.1007/s00018-021-03821-x.
12. Vila MC, Rayavarapu S, Hogarth MW, et al. Mitochondria mediate cell membrane repair and contribute to Duchenne muscular dystrophy. *Cell Death Differ*. 2017;24(2):330–342. https://doi.org/10.1038/cdd.2016.127.
13. Mareedu S, Million ED, Duan D, Babu GJ. Abnormal calcium handling in duchenne muscular dystrophy: mechanisms and potential therapies. *Front Physiol*. 2021;12, 647010. https://doi.org/10.3389/fphys.2021.647010.
14. Bez Batti Angulski A, Hosny N, Cohen H, et al. Duchenne muscular dystrophy: disease mechanism and therapeutic strategies. *Front Physiol*. 2023;14, 1183101. https://doi.org/10.3389/fphys.2023.1183101.
15. Allen DG, Whitehead NP, Froehner SC. Absence of dystrophin disrupts skeletal muscle signaling: roles of Ca2+, reactive oxygen species, and nitric oxide in the development of muscular dystrophy. *Physiol Rev*. 2016;96(1):253–305. https://doi.org/10.1152/physrev.00007.2015.
16. Mohiuddin M, Lee NH, Choi JJ, et al. The muscle stem cell mediates remodeling of skeletal muscle mitochondrial networks. *FASEB J*. 2020;34(S1):1. https://doi.org/10.1096/fasebj.2020.34.s1.04321, 1.
17. Carlson CG. Does the pathogenic sequence of skeletal muscle degeneration in duchenne muscular dystrophy begin and end with unrestrained satellite cell activation? *Muscles*. 2022;1(1):75–81. https://doi.org/10.3390/muscles1010008.
18. Kodippili K, Rudnicki MA. Satellite cell contribution to disease pathology in Duchenne muscular dystrophy. *Front Physiol*. 2023;14, 1180980. https://doi.org/10.3389/fphys.2023.1180980.
19. Giuliani G, Rosina M, Reggio A. Signaling pathways regulating the fate of fibro/adipogenic progenitors (FAPs) in skeletal muscle regeneration and disease. *FEBS J*. 2022;289(21):6484–6517. https://doi.org/10.1111/febs.16080.
20. Chen W, You W, Valencak TG, Shan T. Bidirectional roles of skeletal muscle fibro-adipogenic progenitors in homeostasis and disease. *Ageing Res Rev*. 2022;80, 101682. https://doi.org/10.1016/j.arr.2022.101682.
21. Winter L, Kustermann M, Ernhofer B, Höger H, Bittner RE, Schmidt WM. Proteins implicated in muscular dystrophy and cancer are functional constituents of the centrosome. *Life Sci Alliance*. 2022;5(11), .e202201367. https://doi.org/10.26508/lsa.202201367.
22. Bassett DI, Currie PD. The zebrafish as a model for muscular dystrophy and congenital myopathy. *Hum Mol Genet*. 2003;12:R265–R270. https://doi.org/10.1093/HMG/DDG279.
23. Li M, Andersson-Lendahl M, Sejersen T, Arner A. Muscle dysfunction and structural defects of dystrophin-null sapje mutant zebrafish larvae are rescued by ataluren treatment. *FASEB J*. 2014;28(4):1593–1599. https://doi.org/10.1096/FJ.13-240044.
24. Singh J, Patten SA. Modeling neuromuscular diseases in zebrafish. *Front Mol Neurosci*. 2022;15, 1054573. https://doi.org/10.3389/fnmol.2022.1054573.
25. Keenan SR, Currie PD. The developmental phases of zebrafish myogenesis. *J Dev Biol*. 2019;7(2), 12. https://doi.org/10.3390/JDB7020012.
26. Bassett DI, Bryson-Richardson RJ, Daggett DF, Gautier P, Keenan DG, Currie PD. Dystrophin is required for the formation of stable muscle attachments in the zebrafish embryo. *Development*. 2003;130(23):5851–5860. https://doi.org/10.1242/DEV.00799.
27. Widrick JJ, Alexander MS, Sanchez B, et al. Muscle dysfunction in a zebrafish model of Duchenne muscular dystrophy. *Physiol Genom*. 2016;48(11):850–860. https://doi.org/10.1152/PHYSIOLGENOMICS.00088.2016.
28. Tucker SK, Ghosal R, Swartz ME, Zhang S, Eberhart JK. Correction: zebrafish raptor mutation inhibits the activity of mTORC1, inducing craniofacial defects due to autophagy-induced neural crest cell death. *Development*. 2024;151(8), dev202900. https://doi.org/10.1242/dev.202900. Erratum for: Development. 2024;151(6):dev202216. doi: 10.1242/dev.202216.
29. Lund-Ricard Y, Cormier P, Morales J, Boutet A. Mtor signaling at the crossroad between metazoan regeneration and human diseases. *Int J Mol Sci*. 2020;21(8), 2718. https://doi.org/10.3390/IJMS21082718.
30. Frank DF, Miller GW, Connon RE, Geist J, Lein PJ. Transcriptomic profiling of mTOR and ryanodine receptor signaling molecules in developing zebrafish in the absence and presence of PCB 95. *PeerJ*. 2017;5(11), e4106. https://doi.org/10.7717/PEERJ.4106.
31. Sengupta K, Kolla JN, Krishnaraju AV, et al. Cellular and molecular mechanisms of anti-inflammatory effect of Aflapin: a novel Boswellia serrata extract. *Mol Cell Biochem*. 2011;354(1–2):189–197. https://doi.org/10.1007/S11010-011-0818-1.
32. Xiao Y, Zhou Y, Xiong Z, et al. Involvement of JNK in the embryonic development and organogenesis in Zebrafish. *Marine Biotechnol*. 2013;15(6):716–725. https://doi.org/10.1007/s10126-013-9520-5.
33. Tao T, Shi H, Huang D, Peng J. Def functions as a cell autonomous factor in organogenesis of digestive organs in zebrafish. *PLoS One*. 2013;8(4), e58858. https://doi.org/10.1371/journal.pone.0058858.
34. Relaix F, Bencze M, Borok MJ, et al. Perspectives on skeletal muscle stem cells. *Nat Commun*. 2021;12(1):692. https://doi.org/10.1038/s41467-020-20760-6.
35. Kharraz Y, Guerra J, Pessina P, Serrano AL, Muñoz-Cánoves P. Understanding the process of fibrosis in Duchenne muscular dystrophy. *Biomed Res Int*. 2014;2014, 965631. https://doi.org/10.1155/2014/965631.
36. Wang X, Chen J, Homma ST, et al. Diverse effector and regulatory functions of fibro/adipogenic progenitors during skeletal muscle fibrosis in muscular dystrophy. *iScience*. 2023;26(1), 105775. https://doi.org/10.1016/j.isci.2022.105775.
37. Rodriguez J, Vernus B, Chelh I, et al. Myostatin and the skeletal muscle atrophy and hypertrophy signaling pathways. *Cell Mol Life Sci*. 2014;71(22):4361–4371. https://doi.org/10.1007/s00018-014-1689-x.
38. Der Vartanian A, Quétin M, Michineau S, et al. PAX3 Confers functional heterogeneity in skeletal muscle stem cell responses to environmental stress. *Cell Stem Cell*. 2019;24(6):958–973.e9. https://doi.org/10.1016/j.stem.2019.03.019.
39. de Morree A, Klein JDD, Gan Q, et al. Alternative polyadenylation of Pax3 controls muscle stem cell fate and muscle function. *Science*. 2019;366(6466):734–738. https://doi.org/10.1126/science.aax1694.
40. McKinsey TA, Zhang CL, Olson EN. MEF2: a calcium-dependent regulator of cell division, differentiation and death. *Trends Biochem Sci*. 2002;27(1):40–47. https://doi.org/10.1016/s0968-0004(01)02031-x.
41. Cenik BK, Garg A, McAnally JR, et al. Severe myopathy in mice lacking the MEF2/SRF-dependent gene leiomodin-3. *J Clin Invest*. 2015;125(4):1569–1578. https://doi.org/10.1172/JCI80115.
42. Rodríguez C, Timóteo-Ferreira F, Minchiotti G, Brunelli S, Guardiola O. Cellular interactions and microenvironment dynamics in skeletal muscle regeneration and disease. *Front Cell Dev Biol*. 2024;12, 1385399. https://doi.org/10.3389/FCELL.2024.1385399/XML.
43. Moro E, Vettori A, Porazzi P, et al. Generation and application of signaling pathway reporter lines in zebrafish. *Mol Genet Genom*. 2013;288(5–6):231–242. https://doi.org/10.1007/s00438-013-0750-z.
44. Friedrichs M, Wirsdöerfer F, Flohé SB, Schneider S, Wuelling M, Vortkamp A. BMP signaling balances proliferation and differentiation of muscle satellite cell descendants. *BMC Cell Biol*. 2011;12, 26. https://doi.org/10.1186/1471-2121-12-26.
45. Rhoads RP, Flann KL, Cardinal TR, Rathbone CR, Liu X, Allen RE. Satellite cells isolated from aged or dystrophic muscle exhibit a reduced capacity to promote angiogenesis in vitro. *Biochem Biophys Res Commun*. 2013;440(3):399–404. https://doi.org/10.1016/j.bbrc.2013.09.085.
46. Voronova A, Coyne E, Al Madhoun A, et al. Hedgehog signaling regulates MyoD expression and activity. *J Biol Chem*. 2013;288(6):4389–4404. https://doi.org/10.1074/jbc.M112.400184.
47. Nguyen TH, Conotte S, Belayew A, Declèves AE, Legrand A, Tassin A. Hypoxia and Hypoxia-inducible factor signaling in muscular dystrophies: cause and consequences. *Int J Mol Sci*. 2021;22(13), 7220. https://doi.org/10.3390/ijms22137220.
48. Gioftsidi S, Relaix F, Mourikis P. The Notch signaling network in muscle stem cells during development, homeostasis, and disease. *Skelet Muscle*. 2022;12(1):9. https://doi.org/10.1186/s13395-022-00293-w.
49. Norris AM, Appu AB, Johnson CD, et al. Hedgehog signaling via its ligand DHH acts as cell fate determinant during skeletal muscle regeneration. *Nat Commun*. 2023;14(1):3766. https://doi.org/10.1038/s41467-023-39506-1.
50. Stocco A, Smolina N, Sabatelli P, et al. Treatment with a triazole inhibitor of the mitochondrial permeability transition pore fully corrects the pathology of sapje zebrafish lacking dystrophin. *Pharmacol Res*. 2021;165, 105421. https://doi.org/10.1016/j.phrs.2021.105421.
51. Kollias HD, McDermott JC. Transforming growth factor-beta and myostatin signaling in skeletal muscle. *J Appl Physiol (1985)*. 2008;104(3):579–587. https://doi.org/10.1152/japplphysiol.01091.2007.
52. Pipalia TG, Koth J, Roy SD, Hammond CL, Kawakami K, Hughes SM. Cellular dynamics of regeneration reveals role of two distinct Pax7 stem cell populations in larval zebrafish muscle repair. *Dis Model Mech*. 2016;9(6):671–684. https://doi.org/10.1242/dmm.022251.
53. Wen Y, Bi P, Liu W, Asakura A, Keller C, Kuang S. Constitutive Notch activation upregulates Pax7 and promotes the self-renewal of skeletal muscle satellite cells. *Mol Cell Biol*. 2012;32(12):2300–2311. https://doi.org/10.1128/MCB.06753-11.
54. Yamashita AMS, Garay BI, Kim H, et al. Effect of Notch1 signaling on muscle engraftment and maturation from pluripotent stem cells. *Stem Cell Reports*. 2025;20(2), 102396. https://doi.org/10.1016/j.stemcr.2024.102396.
55. Thomas TO, Morgan TM, Burnette WB, Markham LW. Correlation of heart rate and cardiac dysfunction in duchenne muscular dystrophy. *Pediatr Cardiol*. 2012;33(7):1175–1179. https://doi.org/10.1007/S00246-012-0281-0/TABLES/3.
56. Hakimi M, Burnham T, Ramsay J, et al. Electrophysiologic and cardiovascular manifestations of Duchenne and Becker muscular dystrophies. *Heart Rhythm*. 2025;22(1):192–202. https://doi.org/10.1016/J.HRTHM.2024.07.008.
57. Lechner A, Herzig JJ, Kientsch JG, et al. Cardiomyopathy as cause of death in Duchenne muscular dystrophy: a longitudinal observational study. *ERJ Open Res*. 2023;9(5):00176–02023. https://doi.org/10.1183/23120541.00176-2023c.
58. Schara U, Mortier MW. Long-term steroid therapy in duchenne muscular dystrophy-positive results versus side effects. *J Clin Neuromuscul Dis*. 2001;2(4):179–183. https://doi.org/10.1097/00131402-200106000-00002.
59. Fischer R, Porter K, Donovan JM, et al. A mixed-method study exploring patient-experienced and caregiver-reported benefits and side effects of corticosteroid use in duchenne muscular dystrophy. *J Neuromuscul Dis*. 2023;10(4):593–613. https://doi.org/10.3233/JND-221617.

60. Happi Mbakam C, Tremblay JP. Gene therapy for Duchenne muscular dystrophy: an update on the latest clinical developments. *Expert Rev Neurother*. 2023;23(10): 905–920. https://doi.org/10.1080/14737175.2023.2249607.
61. Rind DM. The FDA and gene therapy for duchenne muscular dystrophy. *JAMA*. 2024;331(20):1705–1706. https://doi.org/10.1001/jama.2024.5613.
62. Dumont NA, Wang YX, Von Maltzahn J, et al. Dystrophin expression in muscle stem cells regulates their polarity and asymmetric division. *Nat Med*. 2015;21(12): 1455–1463. https://doi.org/10.1038/nm.3990.
63. Li Y, Li C, Sun Q, et al. Skeletal muscle stem cells modulate niche function in Duchenne muscular dystrophy mouse through YY1-CCL5 axis. *Nat Commun*. 2025; 16(1):1324. https://doi.org/10.1038/s41467-025-56474-w.
64. Onopiuk M, Brutkowski W, Wierzbicka K, et al. Mutation in dystrophin-encoding gene affects energy metabolism in mouse myoblasts. *Biochem Biophys Res Commun*. 2009;386(3):463–466. https://doi.org/10.1016/j.bbrc.2009.06.053.
65. Zulian A, Schiavone M, Giorgio V, Bernardi P. Forty years later: mitochondria as therapeutic targets in muscle diseases. *Pharmacol Res*. 2016;113:563–573. https://doi.org/10.1016/j.phrs.2016.09.043.
66. Chen TH, Koh KY, Lin KMC, Chou CK. Mitochondrial dysfunction as an underlying cause of skeletal muscle disorders. *Int J Mol Sci*. 2022;23(21), 12926. https://doi.org/10.3390/ijms232112926.
67. Moore TM, Lin AJ, Strumwasser AR, et al. Mitochondrial dysfunction is an early consequence of partial or complete dystrophin loss in mdx mice. *Front Physiol*. 2020;11:690. https://doi.org/10.3389/fphys.2020.00690.
68. Vieira NM, Elvers I, Alexander MS, et al. Jagged 1 rescues the duchenne muscular dystrophy phenotype. *Cell*. 2015;163(5):1204–1213. https://doi.org/10.1016/j.cell.2015.10.049.
69. Markham LW, Brinkmeyer-Langford CL, Soslow JH, et al. GRMD cardiac and skeletal muscle metabolism gene profiles are distinct. *BMC Med Genom*. 2017;10 (1):21. https://doi.org/10.1186/s12920-017-0257-2.
70. Gosselin MRF, Mournetas V, Borczyk M, et al. Loss of full-length dystrophin expression results in major cell-autonomous abnormalities in proliferating myoblasts. *Elife*. 2022;11, e75521. https://doi.org/10.7554/eLife.75521.
71. Suárez-Calvet X, Fernández-Simón E, Natera D, et al. Decoding the transcriptome of Duchenne muscular dystrophy to the single nuclei level reveals clinical-genetic correlations. *Cell Death Dis*. 2023;14(9):596. https://doi.org/10.1038/s41419-023-06103-5.
72. Nieves-Rodriguez S, Barthélémy F, Woods JD, et al. Transcriptomic analysis of paired healthy human skeletal muscles to identify modulators of disease severity in DMD. *Front Genet*. 2023;14, 1216066. https://doi.org/10.3389/fgene.2023.1216066.
73. Granet JA, Robertson R, Cusmano AA, et al. Muscle stem cells in Duchenne muscular dystrophy exhibit molecular impairments and altered cell fate trajectories impacting regenerative capacity. *Cell Death Dis*. 2025;16(1):437. https://doi.org/10.1038/s41419-025-07755-1.
74. Li W, Chen M, Zhang L. Muscle stem cell microenvironment and functions in Muscle regeneration. *Biomolecules*. 2025;15(6), 765. https://doi.org/10.3390/biom15060765.
75. Brorson J, Lin L, Wang J, et al. Complementing muscle regeneration—Fibro-adipogenic progenitor and macrophage-mediated repair of elderly human skeletal muscle. *Nat Commun*. 2025;16(1):5233. https://doi.org/10.1038/s41467-025-60627-2.
76. Theret M, Rossi FMV, Contreras O. Evolving roles of muscle-resident fibro-adipogenic progenitors in health, regeneration, neuromuscular disorders, and aging. *Front Physiol*. 2021;12, 673404. https://doi.org/10.3389/fphys.2021.673404.
77. Bozzi M, Sciandra F, Bigotti MG, Brancaccio A. Misregulation of the ubiquitin–Proteasome system and autophagy in muscular dystrophies associated with the dystrophin–Glycoprotein complex. *Cells*. 2025;14(10), 721. https://doi.org/10.3390/cells14100721.
78. Relaix F, Montarras D, Zaffran S, et al. Pax3 and Pax7 have distinct and overlapping functions in adult muscle progenitor cells. *J Cell Biol*. 2006;172(1): 91–102. https://doi.org/10.1083/jcb.200508044.
79. Buckingham M. Skeletal muscle progenitor cells and the role of Pax genes. *C R Biol*. 2007;330(6–7):530–533. https://doi.org/10.1016/j.crvi.2007.03.015.
80. Soblechero-Martín P, Albiasu-Arteta E, Anton-Martinez A, et al. Duchenne muscular dystrophy cell culture models created by CRISPR/Cas9 gene editing and their application in drug screening. *Sci Rep*. 2021;11(1), 18188. https://doi.org/10.1038/s41598-021-97730-5.
81. Gaina G, Popa Gruianu A. Muscular dystrophy: experimental animal models and therapeutic approaches. *Exp Ther Med*. 2021;21(6):610. https://doi.org/10.3892/etm.2021.10042.
82. de Morree A, Rando TA. Regulation of adult stem cell quiescence and its functions in the maintenance of tissue integrity. *Nat Rev Mol Cell Biol*. 2023;24(5):334–354. https://doi.org/10.1038/s41580-022-00568-6.
83. Rugowska A, Starosta A, Konieczny P. Epigenetic modifications in muscle regeneration and progression of Duchenne muscular dystrophy. *Clin Epigenetics*. 2021;13(1):13. https://doi.org/10.1186/s13148- 021-01001-z.
84. Dubinin MV, Talanov EY, Tenkov KS, Starinets VS, Belosludtseva NV, Belosludtsev KN. The effect of deflazacort treatment on the functioning of skeletal muscle mitochondria in duchenne muscular dystrophy. *Int J Mol Sci*. 2020;21(22), 8763. https://doi.org/10.3390/ijms21228763.
85. Nesari V, Balakrishnan S, Nongthomba U. Is the fundamental pathology in Duchenne's muscular dystrophy caused by a failure of glycogenolysis-glycolysis in costameres? *J Genet*. 2023;102(1):13. https://doi.org/10.1007/s12041-022-01410-w.
86. Casati SR, Cervia D, Roux-Biejat P, Moscheni C, Perrotta C, De Palma C. Mitochondria and reactive oxygen species: the therapeutic balance of powers for Duchenne muscular dystrophy. *Cells*. 2024;13(7), 574. https://doi.org/10.3390/cells13070574.
87. Pircher T, Wackerhage H, Aszodi A, et al. Hypoxic signaling in skeletal muscle maintenance and regeneration: a systematic review. *Front Physiol*. 2021;12, 684899. https://doi.org/10.3389/fphys.2021.684899.
88. Yang X, Yang S, Wang C, Kuang S. The hypoxia-inducible factors HIF1α and HIF2α are dispensable for embryonic muscle development but essential for postnatal muscle regeneration. *J Biol Chem*. 2017;292(14):5981–5991. https://doi.org/10.1074/jbc.M116.756312.
89. Stantzou A, Schirwis E, Swist S, et al. BMP signaling regulates satellite cell-dependent postnatal muscle growth. *Development*. 2017;144(15):2737–2747. https://doi.org/10.1242/dev.144089.
90. Valle-Tenney R, Rebolledo D, Acuña MJ, Brandan E. HIF-hypoxia signaling in skeletal muscle physiology and fibrosis. *J Cell Commun Signal*. 2020;14(2): 147–158. https://doi.org/10.1007/s12079-020-00553-8.
91. Thomas GD. Functional muscle ischemia in Duchenne and Becker muscular dystrophy. *Front Physiol*. 2013;4, 381. https://doi.org/10.3389/fphys.2013.00381.
92. Preethy S, Yamamoto N, Osaza S, et al. Re-examination of therapeutic management of muscular dystrophies using a vascular smooth muscle-centered approach. *J Smooth Muscle Res*. 2023;59:67–80. https://doi.org/10.1540/jsmr.59.67.
93. Voronova A, Coyne E, Al Madhoun A, et al. Hedgehog signaling regulates MyoD expression and activity. *J Biol Chem*. 2013;288(6):4389–4404. https://doi.org/10.1074/jbc.M112.400184.
94. Vieira NM, Elvers I, Alexander MS, et al. Jagged 1 rescues the duchenne muscular dystrophy phenotype. *Cell*. 2015;163(5):1204–1213. https://doi.org/10.1016/j.cell.2015.10.049.
95. Kimmel CB, Ballard WW, Kimmel SR, Ullmann B, Schilling TF. Stages of embryonic development of the zebrafish. *Dev Dyn*. 1995;203(3):253–310. https://doi.org/10.1002/aja.1002030302.
96. Mamchaoui K, Trollet C, Bigot A, et al. Immortalized pathological human myoblasts: towards a universal tool for the study of neuromuscular disorders. *Skelet Muscle*. 2011;1, 34. https://doi.org/10.1186/2044-5040-1-34.
97. Cenni V, Sabatelli P, Mattioli E, et al. Lamin A N-terminal phosphorylation is associated with myoblast activation: impairment in Emery-Dreifuss muscular dystrophy. *J Med Genet*. 2005;42(3):214–220. https://doi.org/10.1136/jmg.2004.026112.
98. Schiavone M, Zulian A, Menazza S, et al. Alisporivir rescues defective mitochondrial respiration in Duchenne muscular dystrophy. *Pharmacol Res*. 2017; 125(Pt B):122–131. https://doi.org/10.1016/j.phrs.2017.09.001.
99. Hardwick SA, Chen WY, Wong T, et al. Spliced synthetic genes as internal controls in RNA sequencing experiments. *Nat Methods*. 2016;13(9):792–798. https://doi.org/10.1038/nmeth.3958.
100. Didion JP, Martin M, Collins FS. Atropos: specific, sensitive, and speedy trimming of sequencing reads. *PeerJ*. 2017;5, e3720. https://doi.org/10.7717/peerj.3720.
101. Bray NL, Pimentel H, Melsted P, Pachter L. Near-optimal probabilistic RNA-seq quantification. *Nat Biotechnol*. 2016;34(5):525–527. https://doi.org/10.1038/nbt.3519.
102. Wong T, Deveson IW, Hardwick SA, Mercer TR. ANAQUIN: a software toolkit for the analysis of spike-in controls for next generation sequencing. *Bioinformatics*. 2017;33(11):1723–1724. https://doi.org/10.1093/bioinformatics/btx038.
103. Love MI, Huber W, Anders S. Moderated estimation of fold change and dispersion for RNA-seq data with DESeq2. *Genome Biol*. 2014;15(12):550. https://doi.org/10.1186/s13059-014-0550-8.
104. Zhang Y, Parmigiani G, Johnson WE. ComBat-seq: batch effect adjustment for RNA-seq count data. *NAR Genom Bioinform*. 2020;2(3):lqaa078. https://doi.org/10.1093/nargab/lqaa078.
105. Liao Y, Wang J, Jaehnig EJ, Shi Z, Zhang B. WebGestalt 2019: gene set analysis toolkit with revamped UIs and APIs. *Nucleic Acids Res*. 2019;47(W1):W199–W205. https://doi.org/10.1093/nar/gkz401.
106. Merico D, Isserlin R, Stueker O, Emili A, Bader GD. Enrichment map: a network-based method for gene-set enrichment visualization and interpretation. *PLoS One*. 2010;5(11), e13984. https://doi.org/10.1371/journal.pone.0013984.
107. Montandon M, Currie PD, Ruparelia AA. Examining muscle regeneration in Zebrafish models of muscle disease. *J Vis Exp*. 2021;(167):e62071. https://doi.org/10.3791/62071.
108. Muntean BS, Horvat CM, Behler JH, et al. A comparative study of embedded and anesthetized zebrafish in vivo on myocardiac calcium oscillation and heart muscle contraction. *Front Pharmacol*. 2010;1:139. https://doi.org/10.3389/fphar.2010.00139.